International Journal of Biological Macromolecules 311 (2025) 143932

Contents lists available at ScienceDirect

International Journal of Biological Macromolecules

journal homepage: www.elsevier.com/locate/ijbiomac

Lipid-lowering effects of bile *Arisaema* polysaccharides on high-fat diet-induced hyperlipidemia: An integrated analysis of metabolomics, lipidomics and microbiome

Fa-zhi Su [a], Chen-xi Bai [a], Wen-sen Zhang [a], Meng Liu [a], Biao Li [a], Ming-hao Sun [a], Yu-jia He [a], Yuan-ning Zeng [b], Yan-ping Sun [a], Bing-you Yang [a], Hai-xue Kuang [a,*,1], Qiu-hong Wang [a,b,*,1]

[a] *Key Laboratory of Basic and Application Research of Beiyao (Heilongjiang University of Chinese Medicine), Ministry of Education, Harbin 150040, China*
[b] *School of Traditional Chinese Medicine, Guangdong Pharmaceutical University, Guangzhou 510006, China*

ARTICLE INFO

Keywords:
Bile *Arisaema* polysaccharides
Hyperlipidemia
Metabolic disorders
Gut microbiome
High throughput sequencing

ABSTRACT

Bile *Arisaema*, a traditional Chinese medicine, has been previously identified by our team to possess antipyretic properties attributed to its polysaccharide component. Recently, we have confirmed that bile *Arisaema* played a significantly lipid-lowering effect on hyperlipidemia rats. Building upon this discovery, the present study aimed to investigate the unexplored hypolipidemic potential of its polysaccharide component and elucidate the underlying mechanisms. A soluble polysaccharide fraction devoid of free proteins, named BAPs, was extracted from bile *Arisaema* using a combination of hot water extraction, alcohol precipitation, and the Sevage method. The structural characteristics of BAPs were preliminarily elucidated through monosaccharide composition analysis (mainly composed of glucose), molecular weight distribution (38.74 kDa and 2.87 kDa), and glycosyl linkage analysis via methylation. The results of animal experiment demonstrated that oral administration of BAPs (400 mg/kg/day) for four weeks significantly improved abnormal serum lipid levels, hepatic function and histopathological injury on high-fat diet-induced hyperlipidemia rats. Mechanistically, the results of high throughput sequencing indicated that BAPs intake markedly altered the hepatic and fecal metabolome and lipidome, while also modulating gut microbiota composition and improving intestinal barrier integrity. Spearman's correlation analysis unveiled closely associations between the altered microbes, lipids, metabolites and serum biochemical indicators. Western blotting and qRT-PCR analyses further confirmed that these metabolic improvements were mediated by the regulation of key genes involved in lipid metabolism. Collectively, this study demonstrated that BAP supplementation effectively improved serum lipid profiles in hyperlipidemia rats by modulating metabolic disorders and restoring gut homeostasis.

Abbreviations: ACC, Acetyl CoA Carboxylase; ALT, alanine aminotransferase; ANOVA, analysis of variance; ApoA1, Apolipoprotein A-1; Ara, arabinose; AST, aspartate aminotransferase; BAPs, bile *Arisaema* polysaccharides; Cer, ceramides; CETP, cholesteryl ester transfer protein; CYP7A1, cholesterol 7α-hydroxylase; D-Fru, D-fructose; DG, diacylglycerols; D-Rib, D-ribose; FFA, free fatty acids; FT-IR, fourier transform infrared spectrometry; Fuc, fucose; Gal, galactose; GalA, galacturonic acid; GC–MS, gas chromatography–mass spectrometry; Glc, glucose; GlcA, glucuronic acid; Man, mannose; HDL-C, high-density lipoprotein cholesterol; HMDB, human metabolome database; HMG-CoA, 3-hydroxy-3-methyl glutaryl coenzyme A reductase; HPGPC, high performance gel permeation chromatography; KEGG, Kyoto encyclopedia of genes and genomes; LCAT, Lecithin-cholesterolacyltransferase; LDL-C, low-density lipoprotein cholesterol; LXR-α, liver X receptor alpha; LysoPAs, lysophosphatidic acids; LysoPCs, lysophosphatidylcholines; LysoPEs, lysophosphatidylethanolamines; LysoPGs, lysophosphatidylglycerols; LysoPIs, lysophosphatidylinositols; LysoPSs, lysophosphatidylserines; NAFLD, non-alcoholic fatty liver disease; NMR, nuclear magnetic resonance; OPLS-DA, orthogonal partial least-squares discrimination analysis; ORO, oil red O staining; PA, phosphatidic acid; PC, phosphatidylcholines; PCA, principal component analysis; PE, phosphatidylethanolamines; PG, phosphatidylglycerols; PI, phosphatidylinositols; PPAR-α, peroxisome proliferators-activated receptor alpha; PS, phosphatidylserines; qRT-PCR, quantitative real-time polymerase chain reaction; QC, quality control; Rha, rhamnose; SCFAs, short-chain fatty acids; SREBP2, Sterol-regulatory element-binding protein 2; TC, total cholesterol; TFA, trifluoroacetic acid; TG, triglyceride; UPLC-MS, ultra-high performance liquid chromatography coupled with mass spectrometry; UPLC-Q-TOF-MS, ultra-high performance liquid chromatography-quadrupole-time of flight-mass spectrometry; VIP, variable importance of projection; Xyl, xylose..

* Corresponding authors at: Heilongjiang University of Chinese Medicine, Xiangfang District, Heping Road, No. 24, Harbin 150040, China.
E-mail addresses: hxkuang56@163.com (H.-x. Kuang), qhwang668@sina.com (Q.-h. Wang).
[1] These authors contributed equally to this work.

https://doi.org/10.1016/j.ijbiomac.2025.143932
Received 29 November 2024; Received in revised form 22 April 2025; Accepted 3 May 2025
Available online 9 May 2025

1. Introduction

Hyperlipidemia is a metabolic disorder characterized by elevated levels of total cholesterol (TC), triglycerides (TG), and low-density lipoprotein cholesterol (LDL-C), alongside reduced levels of high-density lipoprotein cholesterol (HDL-C) [1,2]. This condition is closely associated with dysregulated lipid and cholesterol metabolism. Prolonged hyperlipidemia has been implicated in the development of various complications, including atherosclerosis, non-alcoholic steatohepatitis (NASH), and other metabolic disorders [3,4]. The onset of hyperlipidemia is primarily driven by disruptions in lipid metabolism, encompassing imbalances in lipid synthesis, breakdown, and transport [5,6]. These metabolic abnormalities are directly linked to the activity of key regulatory enzymes such as acetyl-CoA carboxylase (ACC) and hydroxymethylglutaryl-CoA reductase (HMGCR), as well as alterations in apolipoprotein ratios [7–9]. In recent years, accumulating evidence has highlighted the crucial role of gut microbiota in the pathogenesis and progression of hyperlipidemia and its associated complications [10,11]. The gut microbiota represents a vast and complex microbial community residing in the gastrointestinal tract. The collective genome of these microbes is estimated to be 100 times larger than the human genome, earning it the designation of the "second genome." [12,13] Studies have demonstrated that gut microbiota plays a pivotal role in regulating host lipid metabolism by influencing cholesterol metabolism in the liver, modulating lipid oxidation in muscle tissue, and regulating lipid storage in adipose tissue. Additionally, gut microbiota is involved in maintaining intestinal epithelial integrity and modulating gut barrier function, both of which are crucial for lipid homeostasis [14,15]. Given the multifaceted role of gut microbiota in lipid metabolism, a deeper understanding of its mechanisms could provide valuable insights into the development of novel lipid-lowering therapeutic strategies and drug targets.

Currently, multi-omics has emerged as a powerful strategy for the comprehensive analysis of genotypic and phenotypic changes in complex biological systems, utilizing mathematical models to integrate diverse datasets [16]. In the context of hyperlipidemia, both disease pathogenesis and therapeutic interventions are influenced by multiple factors across various biological dimensions. Therefore, the integrative application of multi-omics technologies is crucial for gaining a deeper understanding of hyperlipidemia and elucidating the underlying mechanisms of drug action [17,18]. Among these approaches, metabolomics and lipidomics are particularly relevant to biological phenotypes, as they facilitate the identification of small-molecule metabolites that serve as key intermediaries linking phenotypic traits to physiological states [19,20]. By employing these techniques, we can comprehensively capture dynamic metabolic changes in liver tissue and intestinal metabolites, including metabolic biomarkers, lipid profiles, and protein alterations. Given the complexity of gut microbiota and its pivotal role in metabolic regulation, identifying functional microbial communities through high-throughput sequencing remains a significant yet challenging task. High-throughput sequencing methods such as 16S rDNA, 16S rRNA, and metagenomics are widely employed to investigate the composition, evolutionary relationships, and species diversity of intestinal microbiota [21–23]. Notably, metagenomic sequencing enables in-depth functional and genetic analyses beyond what is achievable with 16S sequencing alone. Compared to 16S sequencing, metagenomics offers superior species identification capabilities [24].

Bile *Arisaema* polysaccharides (BAPs) have been identified by our research team as an active constituent in previous studies [25]. However, it is regrettable that these polysaccharides have not yet been fully purified, leading to potential inaccuracies in essential structural information such as molecular weight distribution and glycosidic linkages. Interestingly, we previously found that BAPs exhibited a significant antipyretic effect by restoring metabolic balance and modulating gut microbiota composition, suggesting that this approach could be further explored to uncover other pharmacological activities of BAPs. Furthermore, in an unpublished study conducted by our team, bile *Arisaema* aqueous extract was shown to significantly ameliorate hyperlipidemia in different high-fat diet (HFD)-induced animal models. This finding led us to hypothesize that polysaccharides may be a key bioactive component responsible for the lipid-lowering effects of *Arisaema*, potentially offering a novel therapeutic application for this medicinal plant.

In the present study, we specifically investigated the lipid-lowering effects of BAPs and elucidated their underlying mechanisms in HFD-induced hyperlipidemia rats. To achieve this, we employed a multi-omics approach, integrating metabolomics, lipidomics, and metagenomics, to explore the intricate relationship between host metabolic profiles and gut microbiota composition. Additionally, ELISA, qRT-PCR, and western blotting analyses were performed to validate the regulatory effects of BAPs on key lipid metabolism-related factors. To the best of our knowledge, this is the first study to identify the lipid-lowering potential of BAPs, providing a theoretical foundation for their potential application in metabolic disease management and highlighting their value as a functional medicinal ingredient.

2. Materials and methods

2.1. Materials

Bile *Arisaema* samples (Batch No. 20220501) were purchased from Beijing Tongrentang Bozhou Yinpian Company. The voucher specimens were stored at the Key Laboratory of Basic and Applied Research, Heilongjiang University of Chinese Medicine, Ministry of Education. Monosaccharide standards, including mannose (Man, No. C17D9H77586), rhamnose (Rha, No. H10S9Z69863), galacturonic acid (GalA, No. K02A9B66077), galactose (Gal, No. E1927035), glucose (Glc, No. Q18F10N80946), glucuronic acid (GlcA, No. K14M10S82777), arabinose (Ara, No. S15A10G85850), xylose (Xyl, No. A22S6X3606), fucose (Fuc, No. X29D7Y27768), D-fructose (D-Fru, No. J01J10R89818), and D-ribose (D-Rib, No. H26F10Z81556), were obtained from Borui Sugar Biotechnology Co., Ltd. (Yangzhou, Jiangsu, China). The purity of the above mentioned standards was >98 %. The SPF-grade HFD was provided by Xiao Shu You Tai (Beijing) Biotechnology Co., Ltd. (SCXK-Jing-2023-0010). LC-MS-grade solvents, including formic acid (No. 28905), ammonium formate, methanol (No. R40121), and acetonitrile, were sourced from Thermo Fisher Scientific (Waltham, MA, USA), while isopropanol and methyl tertiary butyl ether were purchased from Merck. Internal standards for targeted lipidomics analysis, including Lyso PC (12:0), Cer (d18:1/4:0), and PC (13:0/13:0), were purchased from Avanti/zzstandard, with purity exceeding 99 %. ELISA kits for rat LCAT (MM-45056R1), HMGCR (MM-20699R1), PPAR-α (MM-0253R1), ApoA1 (MM-0031R1), and CETP (MM-0382R2) were obtained from Jiangsu Meimian Industrial Co., Ltd. (Yancheng, Jiangsu, China).

2.2. Preparation of BAPs

Crude BAPs were extracted and prepared following a method previously described in our laboratory [25]. After precipitation and redissolution, the crude BAPs were purified using the sevage method to remove free proteins. The resulting solution was concentrated under reduced pressure using a rotary evaporator (EYELA N-1300 S, Tokyo Rikakikai Co., Ltd., Japan) and re-dissolved in distilled water. The solution was then dialyzed using dialysis bags (cut-off 3500 Da) in water for 48 h to eliminate impurities. After dialysis, the final products were concentrated and freeze-dried to yield the purified BAPs.

2.3. Characterization of BAPs

The preliminary chemical properties of BAPs were investigated, including monosaccharide composition, molecular weight, and functional group analysis, following methods established in our previous

report [25]. Briefly, 5 mg of freeze-dried BAPs were subjected to a series of chemical modifications, including methylation, hydrolysis, and acetylation, prior to analysis by GC–MS (Agilent, 6890–5973). For the methylation step, the sample was accurately weighed and dissolved in 1 mL anhydrous DMSO. Methylation reagent A was added, and the mixture was sonicated to ensure complete dissolution. Then, methylation reagent B was introduced, and the reaction was conducted in a magnetic stirring water bath at 30 °C for 60 min, followed by termination with ultra-pure water. The methylated product was then hydrolyzed using 2 M trifluoroacetic acid (TFA) for 90 min. After hydrolysis, the residue was dried and re-dissolved in 2 mL of ultra-pure water, followed by reduction with 60 mg of sodium borohydride for 8 h. Neutralization was performed with glacial acetic acid, and acetylation was carried out by adding acetic anhydride and heating the reaction mixture at 100 °C for 60 min. To remove excess acetic anhydride, 3 mL of toluene was added to the reaction mixture, and this step was repeated 4–5 times. Finally, the acetylated product was dissolved in dichloromethane and prepared for GC–MS analysis. The GC–MS analysis was performed using an Agilent 6890–5973 system equipped with an RXI-5 SIL MS chromatographic column (30 m × 0.25 mm × 0.25 μm). The program temperature conditions were as follows: the initial temperature was set at 120 °C, with an increase to 250 °C at a rate of 3 °C/min, followed by a 5-min hold at 250 °C. The injector and detector temperatures were both set to 250 °C, with helium as the carrier gas and a flow rate of 1 mL/min. The obtained results were compared with the standard mass spectrometry library for identification.

2.4. Animal experiment

In this study, healthy male SPF-grade SD rats, aged 8 weeks and weighing 180–220 g, were selected to investigate the hypolipidemic effects of BAPs. The hyperlipidemia rat model was established by administering a HFD, based on preliminary experiments conducted in our laboratory [26–29]. The rats were obtained from Beijing Vital River Laboratory Animal Technology Co., Ltd. (No. SCXK (JING) 2021–0011). The experimental protocol and procedures were approved by the Ethics Committee of Heilongjiang University of Chinese Medicine (No. 2023092207). All animals were housed under SPF-grade conditions at a controlled temperature of 23 ± 2 °C and a humidity level of 50–60 %.

A total of 60 male SD rats underwent a 7-day adaptive feeding period before being randomly assigned to two groups: (I) a control group (n = 10), which received a standard diet, and (II) a model group (n = 50), which was fed a HFD consisting of 10 % lard, 3 % cholesterol, 5 % egg yolk oil, 0.3 % sodium cholate, 5 % butter, and 76.7 % standard beverage. After 28 days of HFD administration, the model rats were randomly subdivided into five experimental groups: hyperlipidemia control group (Model, fed with HFD); positive control group (Positive, fed with HFD and treated once daily with 40 mg/kg fenofibrate); high-dose BAPs group (BAPs-H, fed with HFD and treated once daily with 400 mg/kg BAPs); medium-dose BAPs group (BAPs-M, fed with HFD and treated once daily with 200 mg/kg BAPs), and low-dose BAPs group (BAPs-L, fed with HFD and treated once daily with 100 mg/kg BAPs). The respective treatments were administered via intragastric gavage after the successful establishment of hyperlipidemia. Meanwhile, rats in the control and model groups were gavaged once daily with an equivalent volume of distilled water. The treatment period lasted for 28 consecutive days. The dosage selection and treatment duration were based on previous studies and preliminary experiments conducted by our research team [25,26].

2.5. Sample collection

At the end of the final administration, the rats were weighed, fasted for 12 h, and anesthetized with pentobarbital sodium. Blood, liver, epididymal fat, and fecal samples were then collected. Portions of liver tissue and epididymal fat were fixed in 4 % paraformaldehyde for subsequent histopathological analysis. Serum samples were obtained by centrifugation at 3500 rpm for 15 min and stored at −80 °C for further analysis.

2.6. Serum biochemical analysis

Serum concentrations of TC (Cat #: A111–1-1), TG (Cat #: A110–1-1), LDL-C (Cat #: A113–1-1), HDL-C (Cat #: A112–1-1), ALT (Cat #: C009–1-1), and AST (Cat #: C010–1-1) were measured using commercial biochemical kits (Nanjing Jiancheng Bio-Engineering Institute Co., Ltd., Nanjing, China), following the manufacturer's instructions.

2.7. Pathological evaluation and lipid accumulation analysis

Histopathological changes in liver tissue before and after BAP treatment were assessed using hematoxylin and eosin (H&E) staining. Briefly, liver tissues were fixed in 4 % paraformaldehyde, embedded in paraffin, and sectioned into continuous slices of 5 μm thickness. The sections were then stained with H&E and observed under a microscope at different magnifications to evaluate pathological changes.

Additionally, lipid accumulation in epididymal fat was assessed, as previous studies suggested that lipid-lowering effects could be directly reflected through this indicator [30]. Oil Red O (ORO) staining was performed on frozen epididymal fat sections. Imaging and quantitative analysis of the stained sections were conducted using Image-Pro Plus 6.0 software (Media Cybernetics, USA).

2.8. Untargeted metabolomics analysis

In this study, untargeted metabolomics analyses of liver and fecal samples were performed to preliminarily explore the potential correlation between the liver and intestinal tract. This investigation aimed to elucidate the lipid-lowering mechanism of BAPs through regulation of the gut-liver axis. For sample preparation, 50 mg of liver tissue was accurately weighed and homogenized with 300 μL of extraction reagent (methanol: acetonitrile: water = 2:2:1) to remove proteins. Similarly, 50 mg of fecal samples were weighed and extracted using the same reagent. Following vortex mixing, the samples were incubated at −20 °C for 30 min and subsequently centrifuged at 14,000 rpm at 4 °C for 10 min. From each sample, 10 μL was pooled to generate quality control (QC) samples for liver and feces, respectively. Finally, approximately 200 μL of the supernatant was used for untargeted metabolomics analysis via ultra-performance liquid chromatography–quadrupole time-of-flight mass spectrometry (UPLC-Q-TOF-MS).

As described in our previous report, a Waters ACQUITY UPLC system coupled with a SYNAPT G2-Si Q-TOF MS system (Waters, USA) was employed for metabolite profiling in liver and stool samples. Chromatographic separation was performed using a UPLC HSS T3 column (1.8 μm, 2.1 × 100 mm). The mobile phase consisted of 0.1 % formic acid in water (A) and 0.1 % formic acid in acetonitrile (B). The column temperature was maintained at 35 °C, with a flow rate of 0.3 mL/min. The injection volume was set to 3 μL, and the auto-sampler was maintained at 4 °C. For optimal chromatographic peak separation, the gradient elution program for liver samples was as follows: 0–2.5 min, 5 %–47 % B; 2.5–6.5 min, 47 %–73 % B; 6.5–10.5 min, 73 % ~ 100 % B; 10.5–12 min, 100 % B; 12–13 min, 100 % ~ 5 % B; 13–14 min, 5 % B. Similarly, the optimized gradient elution for stool samples was as follows: 0–3 min, 5 %–35 % B; 3–9 min, 35 %–67 % B; 9–12 min, 67 %–100 % B; 12–13 min, 100 % ~ 5 % B; 13–14 min, 5 % B. Mass spectrometry was performed under electrospray ionization (ESI) in both positive and negative ion modes. The specific MS parameters were as follows: mass-to-charge ratio (m/z) (100–1200 Da); capillary voltage (3.0 kV for positive ion mode, 2.5 kV for negative ion mode); cone voltage (40 V) and collision energy (20–35 V).

Raw data were acquired using MassLynx software (Waters, USA), and subsequent data processing, including peak alignment, noise

reduction, standardization, and normalization, was performed using Progenesis QI software (Waters, USA). Data tables containing retention time, *m/z*, and normalized peak area for each peak in both positive and negative ion modes were obtained. Multivariate statistical analysis was conducted using SIMCA software (version 14.0). Principal component analysis (PCA) and orthogonal partial least-squares discriminant analysis (OPLS-DA) were employed to identify group differences and screen for differential metabolites associated with HFD-induced hyperlipidemia. The reliability of the OPLS-DA model was evaluated based on R^2 and Q^2 values, where an R^2 value closer to 1 and a Q^2 value >0 indicated a robust model.

To identify potential differential metabolites, the variable importance in projection (VIP) values and *p*-values were calculated. According to literature reports, metabolites with a VIP value >1 and a p-value <0.05 were considered to have a significant association with sample classification. Finally, metabolic networks related to the lipid-lowering effects of BAPs in liver and fecal samples were comprehensively analyzed using the MetaboAnalyst 6.0 platform and the Kyoto Encyclopedia of Genes and Genomes (KEGG) database.

2.9. Targeted lipidomics analysis

Targeted lipidomics analysis was performed to identify characteristic lipids and further elucidate the lipid-lowering mechanism of BAP treatment. For lipid extraction, 50 mg of liver tissue was homogenized with an extraction solvent (MTBE: methanol = 3:1, *v*/v), including the internal standard. Water was then added to the homogenate to facilitate lipid extraction, and the supernatant was collected after centrifugation at 13,000 rpm for 10 min. A 200 μL aliquot of the upper phase was concentrated under vacuum, and the residue was re-dissolved in 200 μL of a solution (acetonitrile: isopropanol = 1:1, *v*/v) for subsequent liquid chromatography-mass spectrometry/mass spectrometry (LC-MS/MS) analysis.

The resuspended samples were stored at 4 °C and injected in 2 μL volumes for targeted lipidomics analysis, which was performed using an LC-ESI-QTRAP-MS system (AB SCIEX QTRAP 6500, USA). A Thermo Accucore™ C30 column (2.6 μm, 2.1 mm × 100 mm) was used for liquid chromatography separation. The flow rate was set at 0.35 mL/min, and the column temperature was maintained at 45 °C. The specific gradient elution conditions and mass spectrometry parameters are summarized in Table S1.

2.10. Metagenomics analysis

Metagenomics analysis of fecal samples, including sample extraction, detection, sequencing, and data analysis, was conducted by Wuhan Metware Biotechnology Co., Ltd. DNA purity and integrity were assessed by agarose gel electrophoresis, and DNA concentrations were quantified using a Qubit fluorometer. DNA samples with adequate quality were then fragmented using Covaris ultrasonic fragmentation to achieve an average length of approximately 350 bp. Following fragmentation, a library was constructed through a series of steps, including end-repair, addition of an A-tail, adapter ligation, purification, and PCR amplification. Library quality was evaluated by quantifying the effective concentration using the Q-PCR method. The final library was sequenced using the Illumina PE150 platform. Gene differences were analyzed by metabolic pathway enrichment and cluster analysis, based on the KEGG database [32].

2.11. ELISA kit determination

Liver tissue homogenates were prepared to assess the expression levels of key proteins involved in lipid metabolism, including peroxisome proliferator-activated receptor alpha (PPAR-α), apolipoprotein A1 (ApoA1), lecithin-cholesterol acyltransferase (LCAT), HMGCR, and cholesteryl ester transfer protein (CETP). The protein levels were determined following the manufacturer's instructions using commercially available ELISA kits (rat species, bought from Jiangsu Meimian Industrial Co., Ltd., Yancheng, Jiangsu, China).

2.12. Real-time quantitative PCR determination

The mRNA expression levels of key genes involved in lipid and cholesterol metabolism were determined by qRT-PCR. Total RNA was extracted from liver tissues using the standard RNA extraction method. Specifically, the samples were treated at room temperature for 10 min after adding TRIzol reagent, followed by 200 μL chloroform, vigorous shaking for 15 s, and centrifuged at 12000 rpm for 15 min (4 °C). The upper water phase (400 μL) was transported into a new centrifuge tube, isopropyl alcohol was added in the same volume, placed at −20 °C for 15 min, and centrifuged at 12000 rpm for 10 min. The supernatant was removed, and 1 mL 75 % ethanol was added to wash the RNA precipitation. Then, RNA purity and concentration were determined using NanoDrop 2000. The integrity of RNA was determined by 1.5 % agarose gel electrophoresis. Quantification, reverse transcription, and subsequent quantitative analysis were performed following protocols established in our laboratory [25]. A total of seven genes were analyzed by qRT-PCR, and the corresponding primer sequences are listed in TableS2. All target gene expression levels were normalized to the internal reference gene GAPDH.

2.13. Western blotting analysis

The total protein of brain tissue were extracted using RIPA Lysis and extraction buffer according to the guideline of manufacture. Briefly, the equivalent amounts of protein were loaded on SDS-polyacrylamide gel electrophoresis (SDS-PAGE) and then transfected onto nitrocellulose membranes. Next, the membranes were washed with phosphate buffer solution (PBS) containing 1 ‰ Tween for 30 min after incubation with primary antibodies targeting CYP7A1 (1: 1000, BS-21429R, BIOSS), LXR-α (1: 1000, 79,762, CST), SREBP2 (1: 1000, 28,212–1-AP, Proteintech, Wuhan, China), HMGCR (1: 1000, bsm-52822r, BIOSS), PPAR-α (1: 1000, 66,826–1-Ig, Proteintech, Wuhan, China) and PPAR-γ (1: 1000, GB11164, Servicebio, Wuhan) at 4 °C overnight, then incubated with anti-rabbit IgG-HRP conjugated secondary antibody (1: 20000) for 1 h. The GAPDH (1: 5000, GB15004, Servicebio, Wuhan) was chosen as an internal standard. Finally, the membranes were detected for the visualization of the protein signal with Odyssey® Clx imaging system, the quantitative analysis was achieved using Image Analysis software (Bethesda, MD, USA).

2.14. Spearman correlation analysis

In this study, the integration of multi-omics data from metabolomics, lipidomics, and metagenomics was performed using Spearman correlation analysis. Differential metabolites, lipids, and bacteria identified in relation to the amelioration of hyperlipidemia were selected for correlation analysis. Specifically, liver differential metabolites and lipids were co-analyzed with bacterial species, as the microbiome plays a crucial role in mediating liver metabolic disorders through the gut-liver axis. Additionally, the correlation analysis included bacteria that co-varied with changes in fecal metabolites, since the microbiome can produce and transform various metabolites in the gut. Spearman's correlation coefficient was calculated using GraphPad software, and coefficients greater than or equal to ±0.8 were considered significant [33,34].

2.15. Data processing and statistical analysis

All data were statistically analyzed using GraphPad Prism software (version 8.0, San Diego, CA, USA) and are presented as means ± standard deviations. Differences between groups were assessed using

analysis of variance (ANOVA). Meanwhile, we have included Cohen's d values alongside *P*-values in all relevant statistical analyses to provide a more comprehensive interpretation of the results (as listed in Table S3). Expression levels of serum biochemical markers, relative abundance of gut microbiota, and intensities of metabolites and lipids were examined and visualized. Additionally, underlying correlations among serum biochemical markers, differential metabolites, and gut microbiota were analyzed using Spearman's correlation and presented with correlation coefficients (r) and *p*-values. Statistical significance was considered when the p-value was <0.05.

3. Results

3.1. The basic physicochemical properties of BAPs

BAPs were successfully extracted and purified through a series of procedures, including hot-water extraction, ethanol precipitation, and protein removal using the Sevage method followed by dialysis. The basic physicochemical properties of BAPs were characterized, and the results are summarized in Table 1. The total sugar content of BAPs was found to be 76.8 %, while the total protein content and uronic acid content were 1.39 % and 1.25 %, respectively, as determined using the phenol-H_2SO_4 method, Coomassie Brilliant Blue method, and modified carbazole sulfate method. Monosaccharide composition analysis revealed that BAPs predominantly consist of Ara, Gal, Glc, Man and Xyl, with molar ratios of 0.047, 0.111, 0.740, 0.062 and 0.041, respectively (Fig. 1A). The results of high-performance gel permeation chromatography (HPGPC) analysis indicated that BAPs primarily contained two components, with molecular weights of 3.87×10^4 Da and 2.87×10^3 Da, respectively (Fig. 1B).

Fourier transform infrared spectrometry (FT-IR) was employed to investigate the functional groups of BAPs (Fig. 1C). The observed absorbance peaks were as follows: A broad peak at 3426 cm^{-1} corresponded to the O—H stretching vibration, characteristic of sugars [35]. A peak at 2929 cm^{-1} was attributed to C—H stretching vibration [36], while a peak at 1637 cm^{-1} indicated bound water [37]. Peaks at 1419 cm^{-1}, 1151 cm^{-1}, and 1079 cm^{-1} were identified as C—O stretching vibrations [38,39]. Peaks at 1241 cm^{-1}, 1201 cm^{-1}, and 1029 cm^{-1} represented O—H bending vibrations [40]. The peak at 931 cm^{-1} was indicative of the asymmetric ring stretching vibration of the pyranose ring, while the peak at 844 cm^{-1} corresponded to the C—H angular oscillation of the α-end group of the pyranose ring [41]. A peak at 761 cm^{-1} was assigned to the symmetric ring stretching vibration of the pyranose ring.

Table 1
Physicochemical characterization of BAPs.

	BAPs
Chemical composition (%)	
Total sugar[a]	76.8
Protein[b]	1.39
Uronic acid[c]	1.25
Monosaccharide composition (molar ratio)	
Ara	0.047
Gal	0.111
Glc	0.740
Man	0.062
Xyl	0.041
Molecular weight distribution (Da)	
Peak 1	
Mp-1	38,356
Mw-1	38,740
Mn-1	37,454
Peak 2	
Mp-2	2763
Mw-2	2867
Mn-2	2751

[a] Determined by phenol-H_2SO_4 method.
[b] Determined by coomassie brilliant blue method.
[c] Determined by modified carbazole sulfate method.

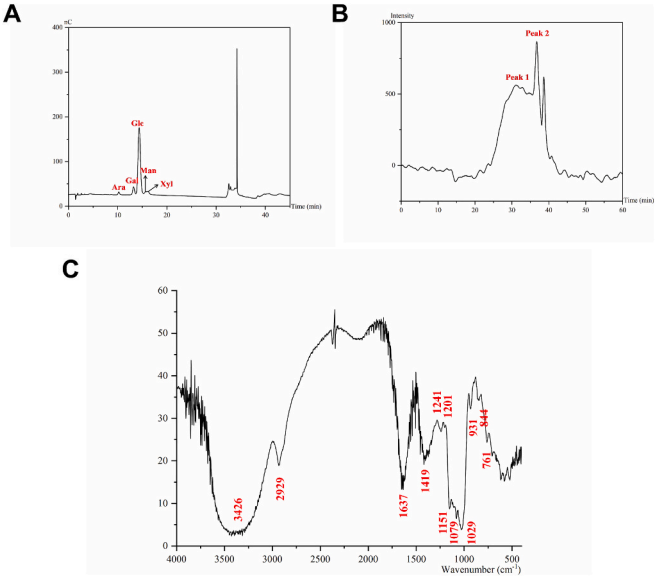

Fig. 1. The preliminary chemical properties of BAPs. (A) Ion chromatograms (IC) of BAPs. (B) HPGPC chromatograms of molecular weight distribution. (C) FT-IR spectrum of BAPs.

To further elucidate the sugar residue composition, GC–MS was employed. The total ion chromatogram and peak annotations for each sugar residue are shown in Fig. 2 and Table 2, alongside the corresponding mass spectrometry bar graphs. The results revealed that the glycosidic bonds in BAPs contain the following sugar residues: T-Araf (2.2 %, mol%), Xylp (3.7 %, mol%), 1,5-Araf (2.2 %, mol%), Glcp (13 %, mol%), Manp (1.1 %, mol%), 1,2-Manp (1.1 %, mol%), 1,3-Glcp (1.7 %, mol%), 1,4-Galp (10.4 %, mol%), 1,4-Glcp (52.8 %, mol%), 1,6-Glcp (2.5 %, mol%), 1,3,4-Glcp (2.6 %, mol%), 1,2,4-Manp (0.9 %, mol%), and 1,4,6-Glcp (5.1 %, mol%). These findings suggest that the main chain of BAPs consists of repeating 1,4-glucosyl units, with branching

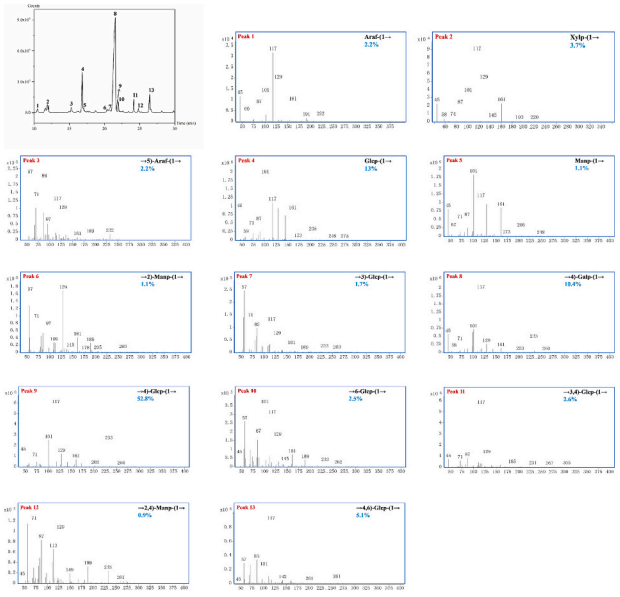

Fig. 2. Methylation analysis of BAPs. (A) GC–MS chromatograms of methylation analysis of BAPs. (B) The EI-MS spectra of peak 1–13.

Table 2
Methylation results of BAPs.

Methylated products	Type of linkage	Major mass fragments (*m/z*)	Molar ratio
2,3,5-Me_3-Araf	Araf-(1→	45,71,87,101,117,129,145,161	0.022
2,3,5-Me_3-Xylp	Xylp-(1→	45,71,87,101,117,129,145,161	0.037
2,3-Me_2-Araf	→5)-Araf-(1→	45,71,87,99,101,117,129,161,189	0.022
2,3,4,6-Me_4-Glcp	Glcp-(1→	45,71,87,101,117,129,145,161,205	0.130
2,3,4,6-Me_4-Manp	Manp-(1→	45,71,87,101,117,129,145,161,205	0.011
3,4,6-Me_3-Manp	→2)-Manp-(1→	45,87,129,161,189	0.011
2,4,6-Me_3-Glcp	→3)-Glcp-(1→	45,87,99,101,117,129,161,173,233	0.017
2,3,6-Me_3-Galp	→4)-Galp-(1→	45,87,99,101,113,117,129,131,161,173,233	0.104
2,3,6-Me_3-Glcp	→4)-Glcp-(1→	45,87,99,101,113,117,129,131,161,173,233	0.528
2,3,6-Me_3-Manp	→4)-Manp-(1→	45,87,99,101,113,117,129,131,161,173,233	0.008
2,3,4-Me_3-Glcp	→6-Glcp-(1→	45,87,99,101,117,129,161,189,233	0.025
2,6-Me_2-Glcp	→3,4)-Glcp-(1→	45,87,97,117,159,185	0.026
3,6-Me_2-Manp	→2,4)-Manp-(1→	45,87,99,117,129,145,159	0.009
2,3-Me_2-Glcp	→4,6)-Glcp-(1→	45,71,85,87,99,101,117,127,159,161,201,261	0.051

points at 1,3,4-linkage, 1,2,4-linkage, and 1,4,6-linkage, indicating that BAPs possess a branched structure with distinct branches.

3.2. Effect of BAPs on body weight gain in rats with hyperlipidemia

In this study, the body weight of rats was recorded weekly for a period of 8 consecutive weeks (Fig. 3A). As shown in Fig. 3B and Table 3, there was no significant difference in body weight gain among the groups during the first three weeks of modeling, indicating that the random grouping was appropriate. However, by the fourth week, the body weight of the rats in the HFD model group increased significantly compared to the control group ($P < 0.05$, $P < 0.01$). This observation, in conjunction with the blood lipid levels of the rats in the fourth week, led to the determination that the administration of BAPs at different dosages should begin at this point. Interestingly, during the first two weeks of treatment, the different dosages of BAPs did not significantly affect body weight gain compared to the model group ($P > 0.05$). However, by the 7th and 8th weeks, rats in the BAPs-H, BAPs-M, and BAPs-L groups exhibited significantly lower body weight compared to the model group ($P < 0.05$, $P < 0.01$). Notably, there was no significant difference in body weight reduction among the three BAP dose groups, suggesting that BAPs exert an inhibitory effect on body weight gain, irrespective of the dosage.

3.3. Effect of BAPs on blood lipid levels in hyperlipidemia rats

Biochemical analyses were performed to evaluate the lipid-lowering effects of different dosages of BAPs. The changes in blood lipid profiles

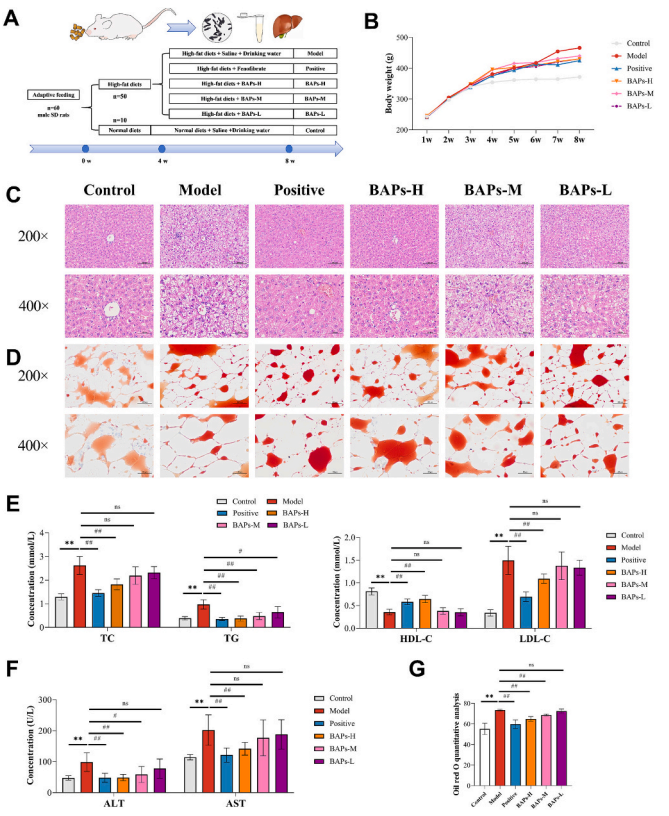

Fig. 3. Effect of BAPs on high-fat diet-induced hyperlipidemia rats. (A) Experimental design for assessing the lipid-lowering effect of BAPs. (B) Body weight changes in hyperlipidemia rats before and after BAPs treatment ($n = 10$). (C) H&E staining of liver tissues from hyperlipidemia rats treated with BAPs (200× and 400×). (D) Oil Red O staining of epididymis fat tissues from hyperlipidemia rats treated with BAPs (200× and 400×). (E) Effects of BAPs supplementation on blood lipid level in high-fat diet-induced hyperlipidemia rats (n = 10). (F) Effects of BAPs supplementation on biochemical indicators of liver functions in high-fat diet-induced hyperlipidemia rats (n = 10). (G) Quantitative analysis of lipid accumulation in epididymis fat tissues before and after BAP treatment. n = 10, data are expressed as the mean ± SD. $^{*}P < 0.05$, $^{**}P < 0.01$, compared with the Control group; $^{\#}P < 0.05$, $^{\#\#}P < 0.01$, compared with the Model group.

and liver function indicators are shown in Fig. 3E-F. After 8 weeks of a HFD, the levels of TC, TG, and LDL-C were significantly elevated in the hyperlipidemic rats ($P < 0.01$), while the HDL-C level was notably lower compared to the control group ($P < 0.01$). Treatment with fenofibrate and high-dose BAPs significantly decreased serum TC, TG, and LDL-C levels ($P < 0.01$), while also increasing HDL-C levels ($P < 0.01$). In contrast, rats treated with medium and low doses of BAPs only showed a decrease in serum TG levels ($P < 0.01$, $P < 0.05$), with no significant effects observed on other lipid parameters. These findings suggest that high-dose BAPs are the most effective in reducing blood lipid levels. Additionally, the potential hepatoprotective effects of BAPs in HFD-induced hyperlipidemia were also investigated (Fig. 3F). The results revealed that serum levels of ALT and AST were significantly higher in the model rats compared to the control group ($P < 0.01$). Following 4 weeks of high-dose BAP treatment, both ALT and AST levels significantly decreased ($P < 0.01$) compared to the model group. However, medium and low doses of BAPs only slightly reduced serum ALT and AST levels ($P > 0.05$ compared to the model group). This suggests that high-dose BAPs play a critical role in ameliorating HFD-induced liver injury.

Table 3
Effect of BAPs consumption on body weight in high-fat diet-induced hyperlipidemia rats.

No.	Control	Model	Positive	BAPs-H	BAPs-M	BAPs-L
1w	243.30 ± 5.39	241.56 ± 5.91	241.69 ± 6.45	246.14 ± 7.93	245.85 ± 5.89	241.10 ± 6.02
2w	297.51 ± 15.71	304.88 ± 12.60	300.50 ± 8.73	301.13 ± 14.22	301.50 ± 13.92	298.50 ± 16.52
3w	339.31 ± 21.19	346.39 ± 16.04	337.80 ± 12.21	348.36 ± 26.08	341.96 ± 23.37	341.05 ± 18.64
4w	354.10 ± 17.62	380.56 ± 18.76*	375.65 ± 16.88*	395.88 ± 28.91**	394.79 ± 20.86**	374.90 ± 13.17*
5w	361.50 ± 12.15	400.98 ± 14.24	393.28 ± 15.42	402.58 ± 24.70	415.29 ± 35.97	399.80 ± 25.88
6w	364.03 ± 13.09	416.98 ± 9.44	413.35 ± 27.90	409.90 ± 29.50	418.38 ± 36.96	405.21 ± 37.01
7w	364.54 ± 17.33	454.29 ± 20.89**	411.05 ± 39.78$^{\#}$	421.74 ± 13.62$^{\#\#}$	430.76 ± 44.69	420.20 ± 18.41$^{\#\#}$
8w	371.55 ± 14.43	465.89 ± 26.99**	424.55 ± 24.52$^{\#\#}$	429.80 ± 17.28$^{\#\#}$	439.55 ± 16.88$^{\#}$	430.39 ± 25.20$^{\#}$

Data are expressed as the mean ± SD. *P<0.05, **$P < 0.01$, compared with the Control group; $^{\#}P < 0.05$, $^{\#\#}P < 0.01$, compared with the Model group.

3.4. BAPs ameliorate liver pathological damage and epididymal fat lipid accumulation

Histopathological analysis of liver tissues was performed using H&E staining and high-power microscopy (200× and 400× magnification). As shown in Fig. 3C, no significant pathological changes were observed in the liver of control rats, except for minor lipid accumulation. In contrast, rats fed a HFD for 8 weeks showed severe liver damage, including disorganized hepatic cord arrangement, excessive lipid droplet accumulation, extensive cytoplasmic vacuolization, and pronounced liver steatosis. These results indicate that a HFD leads to fat deposition in the liver, impairing lipid transport and metabolism. Interestingly, treatment with BAPs-H significantly alleviated liver damage, as evidenced by reduced hepatic steatosis, fewer cytoplasmic vacuoles, and intensified cytoplasmic staining. In contrast, the medium- and low-dose BAP treatments showed no significant improvements in liver tissue, suggesting that the lipid-lowering effect of BAPs is dose-dependent, with high-dose BAPs demonstrating the most potent protective effects.

Lipid accumulation in epididymal white fat is another critical indicator for evaluating the lipid-lowering effects of treatments in HFD-induced hyperlipidemia rats. To assess this, ORO staining was performed to visualize and quantify lipid accumulation in epididymal fat tissue (Fig. 3D and G). The results revealed that HFD feeding significantly increased lipid accumulation in epididymal fat compared to control rats ($P < 0.01$). However, treatment with fenofibrate, BAPs-H, and BAPs-M significantly reduced fat accumulation, as indicated by a reduced percentage of the red-stained positive area ($P < 0.01$). In contrast, BAPs-L had little effect on lipid accumulation ($P > 0.05$), consistent with the biochemical analysis results. In conclusion, supplementation with an appropriate dose of BAPs appears to effectively reduce lipid accumulation in both the liver and epididymal fat.

3.5. Effect of BAPs intake on improved liver metabolic disorders

3.5.1. Multivariate statistical analysis

Before identifying potential biomarkers, we conducted a series of multivariate statistical analyses, including unsupervised PCA and supervised OPLS-DA, to examine the clustering patterns among the three groups ($n = 8$). Herein, according to the results of biochemical analysis, in order to reduce the dispersion degree of each group of samples in metabolomics analysis, and enhance the reliability of metabolomics multivariate statistical analysis results. Therefore, for this part of the study, we removed two samples from each group that were more discrete, and used the remaining eight samples for metabolomics study. Firstly, the QC samples from both feces and liver tissue showed tight clustering, as seen in Fig. 4A and E, indicating that the UPLC-Q-TOF-MS system was stable across consecutive injections. This ensured the reliability of the acquired data from fecal and liver samples, making them suitable for subsequent untargeted metabolomics analysis. PCA score plots for fecal and liver samples (Fig. 4B and F) revealed a clear separation between the control and model groups. This indicates that the endogenous metabolite profiles in the feces and liver of the model rats

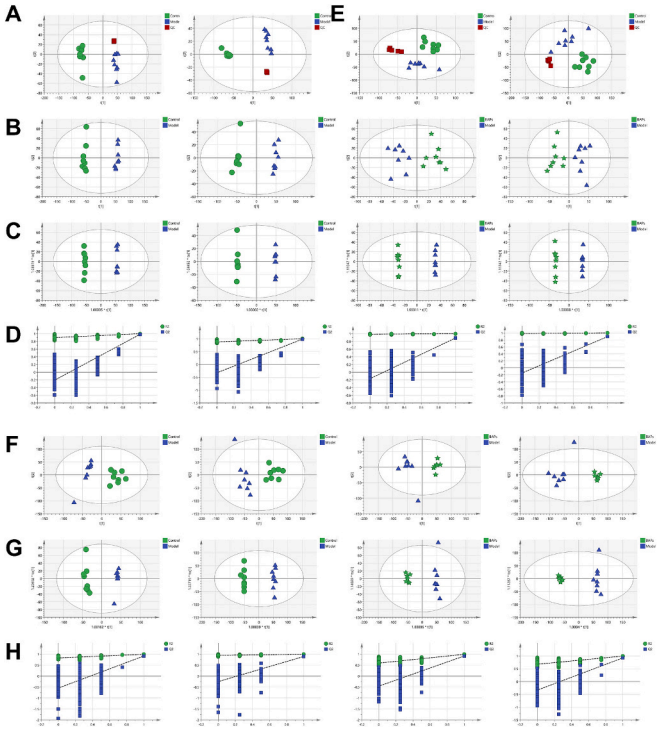

Fig. 4. Multivariate statistical analysis of hyperlipidemia SD rats treated with BAPs-H (liver tissues and fecal samples, $n = 8$). (A) PCA score plot of untargeted fecal metabolism analysis for control, model, and QC samples in both positive and negative ion modes. (B) PCA score plot of untargeted fecal metabolism analysis for control, model, and BAPs-H groups. (C) OPLS-DA model for untargeted fecal metabolism analysis for control, model, and BAPs-H groups. (D) Permutation test of OPLS-DA model for fecal samples. (E) PCA score plot of untargeted liver metabolism analysis for control, model, and QC samples in both positive and negative ion modes. (F) PCA score plot of untargeted liver metabolism analysis for control, model, and BAPs-H groups. (G) OPLS-DA model for untargeted liver metabolism analysis for control, model, and BAPs-H groups. (H) Permutation test of OPLS-DA model for liver samples.

significantly differed from those of the control group, confirming the success of the HFD model for pharmacodynamics studies. Notably, treatment with BAPs-H resulted in a distinct separation of metabolite levels in both feces and liver samples from the model group, highlighting the ability of BAPs-H to substantially improve the metabolic disturbances induced by the HFD. To enhance inter-group separation and improve the accuracy of identifying variables that significantly contribute to classification, we further applied a supervised OPLS-DA model. As illustrated in Fig. 4C and G, a clear separation of variables was observed in all comparisons (control vs. model; model vs. BAPs-H) for both feces and liver samples. A permutation test for the OPLS-DA model was then performed, with results visualized in Fig. 4D and H and summarized in Table 4. The R^2Y values and Q^2 values for the OPLS-

Table 4
The specific parameters of OPLS-DA model and permutation test in the liver samples ($n = 8$) and fecal samples (n = 8).

Source	Group	OPLS-DA			Permutation test	
		R^2X	R^2Y	Q^2	R^2	Q^2
Liver	Con VS Mod P	0.492	0.995	0.89	0.94	−0.253
	Con VS Mod N	0.38	0.99	0.913	0.825	−0.547
	Mod VS BAPs P	0.507	0.993	0.922	0.675	−0.333
	Mod VS BAPs N	0.554	0.99	0.915	0.589	−0.459
Fecal	Con VS Mod P	0.529	0.999	0.986	0.877	−0.325
	Con VS Mod N	0.494	0.999	0.983	0.896	−0.21
	Mod VS BAPs P	0.382	0.999	0.887	0.985	−0.17
	Mod VS BAPs N	0.398	0.999	0.894	0.984	−0.146

DA model in both samples were close to 1, indicating that the model had good predictability and was effective in assessing metabolic changes. Additionally, the Q^2 values from the permutation test were all <0, confirming that the OPLS-DA model was not overfitted. Based on these results, differential metabolites were identified.

3.5.2. Identification of potential biomarkers in different samples

In this section, we identified differential metabolites that significantly contributed to the classification and met the following screening criteria: $P < 0.05$, VIP > 1, and FC ≥ 2 or ≤ 0.5. A total of 51 metabolites in liver tissues were confirmed as potential biomarkers of HFD-induced hyperlipidemia in rats (Table 5 and Fig. 6A). These were identified by analyzing primary and secondary mass spectrometry fragment ion data using Progenesis QI software, and by matching against online databases such as HMDB and KEGG. Compared to control rats, 35 metabolites in the liver were significantly elevated, while 16 metabolites were significantly reduced in the model rats. After intervention with BAPs-H, 39 metabolites showed a tendency to revert to normal levels, while 12 metabolites continued to either increase or decrease. These findings suggest that BAPs-H has the potential to regulate metabolic disturbances

Table 5
The significant differential hepatic metabolites among all groups under positive and negative ion modes.

No.	Compound ID	HMDB ID	Formula	m/z	Trend 1	Trend 2
1	4-Pyridoxic acid	HMDB0000017	$C_8H_9NO_4$	201.0874	↑	↓
2	Betaine	HMDB0000043	$C_5H_{11}NO_2$	118.0866	↑	↑
3	Epinephrine	HMDB0000068	$C_9H_{13}NO_3$	201.1235	↑	↓
4	Glycerophosphocholine	HMDB0000086	$C_8H_{20}NO_6P$	258.1107	↑	↓
5	Glycerylphosphorylethanolamine	HMDB0000114	$C_5H_{14}NO_6P$	238.0454	↑	↓
6	L-Tyrosine	HMDB0000158	$C_9H_{11}NO_3$	182.0819	↑	↓
7	L-Proline	HMDB0000162	$C_5H_9NO_2$	116.0708	↑	↓
8	Phenylpyruvic acid	HMDB0000205	$C_9H_8O_3$	182.0819	↑	↑
9	Palmitic acid	HMDB0000220	$C_{16}H_{32}O_2$	239.2374	↑	↑
10	L-Palmitoylcarnitine	HMDB0000222	$C_{23}H_{45}NO_4$	438.2980	↑	↑
11	Pyridoxine	HMDB0000239	$C_8H_{11}NO_3$	187.1077	↑	↓
12	Riboflavin	HMDB0000244	$C_{17}H_{20}N_4O_6$	377.1464	↓	↑
13	Sphingosine	HMDB0000252	$C_{18}H_{37}NO_2$	300.2909	↑	↓
14	Sphinganine	HMDB0000269	$C_{18}H_{39}NO_2$	284.2952	↑	↓
15	Urocanic acid	HMDB0000301	$C_6H_6N_2O_2$	156.0772	↑	↓
16	Vitamin A	HMDB0000305	$C_{20}H_{30}O$	269.2273	↓	↑
17	L-Methionine	HMDB0000696	$C_5H_{11}NO_2S$	150.0589	↑	↓
18	L-Valine	HMDB0000883	$C_5H_{11}NO_2$	118.0866	↑	↓
19	Arachidonic acid	HMDB0001043	$C_{20}H_{32}O_2$	287.2378	↑	↓
20	Retinal	HMDB0001358	$C_{20}H_{28}O$	267.2118	↓	↑
21	(*R*)-lipoic acid	HMDB0001451	$C_8H_{14}O_2S_2$	207.0511	↑	↑
22	Metanephrine	HMDB0004063	$C_{10}H_{15}NO_3$	180.1022	↑	↓
23	Carnosine	HMDB0000033	$C_9H_{14}N_4O_3$	225.0987	↑	↓
24	Taurocholic acid	HMDB0000036	$C_{26}H_{45}NO_7S$	514.2834	↓	↑
25	Glycocholic acid	HMDB0000138	$C_{26}H_{43}NO_6$	464.3012	↓	↑
26	Hypoxanthine	HMDB0000157	$C_5H_4N_4O$	171.0076	↓	↑
27	L-Dopa	HMDB0000181	$C_9H_{11}NO_4$	196.0619	↑	↓
28	Pantothenic acid	HMDB0000210	$C_9H_{17}NO_5$	218.1042	↓	↑
29	Porphobilinogen	HMDB0000245	$C_{10}H_{14}N_2O_4$	225.0885	↓	↓
30	Allodeoxycholic acid	HMDB0000478	$C_{24}H_{40}O_4$	391.2845	↑	↓
31	Capric acid	HMDB0000511	$C_{10}H_{20}O_2$	217.1965	↓	↑
32	Chenodeoxycholic acid	HMDB0000518	$C_{24}H_{40}O_4$	391.2845	↑	↓
33	Cholic acid	HMDB0000619	$C_{24}H_{40}O_5$	407.2807	↓	↓
34	Deoxycholic acid	HMDB0000626	$C_{24}H_{40}O_4$	391.2845	↑	↓
35	Deoxycholic acid glycine conjugate	HMDB0000631	$C_{26}H_{43}NO_5$	448.3064	↓	↓
36	Lithocholic acid glycine conjugate	HMDB0000698	$C_{26}H_{43}NO_4$	414.3011	↓	↑
37	Taurodeoxycholic acid	HMDB0000896	$C_{26}H_{45}NO_6S$	498.2883	↑	↓
38	Prostaglandin E2	HMDB0001220	$C_{20}H_{32}O_5$	351.2180	↓	↑
39	5,6-Epoxy-8,11,14-eicosatrienoic acid	HMDB0002190	$C_{20}H_{32}O_3$	319.2282	↑	↑
40	8,9-Epoxyeicosatrienoic acid	HMDB0002232	$C_{20}H_{32}O_3$	319.2282	↑	↑
41	14,15-DiHETrE	HMDB0002265	$C_{20}H_{34}O_4$	337.2388	↑	↓
42	8,9-DiHETrE	HMDB0002311	$C_{20}H_{34}O_4$	337.2388	↑	↓
43	11,12-DiHETrE	HMDB0002314	$C_{20}H_{34}O_4$	337.2388	↑	↓
44	5,6-DHET	HMDB0002343	$C_{20}H_{34}O_4$	337.2388	↑	↓
45	6-Keto-prostaglandin F1a	HMDB0002886	$C_{20}H_{34}O_6$	351.2180	↑	↑
46	Retinyl ester	HMDB0003598	$C_{20}H_{30}O_2$	301.2175	↓	↓
47	11-Dehydro-thromboxane B2	HMDB0004242	$C_{20}H_{32}O_6$	367.2136	↓	↑
48	12(*S*)-HPETE	HMDB0004243	$C_{20}H_{32}O_4$	317.2132	↑	↓
49	15(*S*)-HPETE	HMDB0004244	$C_{20}H_{32}O_4$	317.2132	↑	↓
50	3a-Hydroxy-5b-pregnane-20-one	HMDB0006759	$C_{21}H_{34}O_2$	635.5037	↓	↑
51	12-KETE	HMDB0013633	$C_{20}H_{30}O_3$	317.2132	↑	↓

Trend 1 indicated the changing information of differential metabolites between control and model groups; Trend 2 indicated the changing information of differential metabolites between model and BAPs-H groups.

in hyperlipidemia rats to some extent. Similarly, a total of 55 metabolites in fecal samples were identified as potential biomarkers (Table 6 and Fig. 5A) based on the same screening criteria. In the HFD-induced hyperlipidemia rats, 29 metabolites were significantly elevated, and 26 metabolites were significantly decreased compared to normal rats. After BAPs-H treatment, 31 metabolites showed a reversal in their expression levels, while 24 metabolites did not exhibit any such reversal. These results indicate that BAPs-H administration significantly modulates metabolic disorders in the gut, although the precise relationship with gut microbiota requires further investigation.

3.5.3. *Metabolic pathway enrichment analysis of potential biomarkers*

To gain insight into the biological functions of the identified potential biomarkers, we performed a metabolic pathway enrichment analysis using the KEGG database via the MetaboAnalyst platform. The results of this analysis (Fig. 5B-D, Fig. 6B-D) revealed that the fecal biomarkers were involved in 17 perturbed metabolic pathways, including arachidonic acid metabolism, phenylalanine metabolism, glycine, serine and threonine metabolism, pyrimidine metabolism, and nicotinate and nicotinamide metabolism, among others. Similarly, the hepatic biomarkers were implicated in pathways such as retinol metabolism, arachidonic acid metabolism, phenylalanine, tyrosine, and tryptophan biosynthesis, riboflavin metabolism, phenylalanine metabolism, tyrosine metabolism, histidine metabolism, and sphingolipid metabolism. Conclusively, metabolic variations among comparisons of model vs. BAPs-H were investigated in both liver and fecal samples, it

Table 6
The significant differential fecal metabolites among all groups under positive and negative ion modes.

No.	Compound ID	Formula	HMDB ID	m/z	Trend 1	Trend 2
1	Bilirubin	$C_{33}H_{36}N_4O_6$	HMDB0000054	585.2701	↑	↓
2	Deoxyadenosine	$C_{10}H_{13}N_5O_3$	HMDB0000101	252.1088	↑	↓
3	Phenylpyruvic acid	$C_9H_8O_3$	HMDB0000205	182.0806	↑	↓
4	L-Palmitoylcarnitine	$C_{23}H_{45}NO_4$	HMDB0000222	400.3411	↑	↑
5	Sphingosine	$C_{18}H_{37}NO_2$	HMDB0000252	282.2781	↓	↑
6	Tryptamine	$C_{10}H_{12}N_2$	HMDB0000303	161.1069	↓	↑
7	Chenodeoxycholic acid	$C_{24}H_{40}O_4$	HMDB0000518	410.3269	↓	↓
8	Isoursodeoxycholic acid	$C_{24}H_{40}O_4$	HMDB0000686	410.3269	↓	↓
9	Hyodeoxycholic acid	$C_{24}H_{40}O_4$	HMDB0000733	410.3269	↓	↓
10	L-Valine	$C_5H_{11}NO_2$	HMDB0000883	100.0760	↑	↑
11	Ursocholic acid	$C_{24}H_{40}O_5$	HMDB0000917	426.3204	↑	↓
12	Ursodeoxycholic acid	$C_{24}H_{40}O_4$	HMDB0000946	410.3269	↓	↓
13	Arachidonic acid	$C_{20}H_{32}O_2$	HMDB0001043	287.2357	↑	↓
14	Lathosterol	$C_{27}H_{46}O$	HMDB0001170	425.3039	↑	↓
15	24-Hydroxycholesterol	$C_{27}H_{46}O_2$	HMDB0001419	425.3408	↑	↓
16	D-Urobilinogen	$C_{33}H_{42}N_4O_6$	HMDB0004158	591.3170	↑	↓
17	Deoxyuridine	$C_9H_{12}N_2O_5$	HMDB0000012	227.0669	↑	↓
18	Cellobiose	$C_{12}H_{22}O_{11}$	HMDB0000055	341.1082	↑	↓
19	Deoxyinosine	$C_{10}H_{12}N_4O_4$	HMDB0000071	251.0786	↓	↓
20	D-Xylose	$C_5H_{10}O_5$	HMDB0000098	185.0228	↓	↓
21	Homovanillic acid	$C_9H_{10}O_4$	HMDB0000118	241.0872	↓	↓
22	L-Serine	$C_3H_7NO_3$	HMDB0000187	164.0730	↑	↓
23	Inosine	$C_{10}H_{12}N_4O_5$	HMDB0000195	267.0733	↑	↓
24	N-Acetyl-D-glucosamine	$C_8H_{15}NO_6$	HMDB0000215	256.0595	↑	↓
25	Thymine	$C_5H_6N_2O_2$	HMDB0000262	251.0781	↓	↓
26	Thymidine	$C_{10}H_{14}N_2O_5$	HMDB0000273	241.0833	↑	↓
27	Vanillylmandelic acid	$C_9H_{10}O_5$	HMDB0000291	197.0464	↑	↑
28	Uridine	$C_9H_{12}N_2O_6$	HMDB0000296	243.0625	↑	↓
29	16-a-Hydroxypregnenolone	$C_{21}H_{32}O_3$	HMDB0000315	331.2273	↓	↑
30	18-Hydroxycorticosterone	$C_{21}H_{30}O_5$	HMDB0000319	361.2028	↓	↓
31	Arabinonic acid	$C_5H_{10}O_6$	HMDB0000539	225.0779	↓	↑
32	Galactonic acid	$C_6H_{12}O_7$	HMDB0000565	195.0515	↑	↓
33	Dodecanedioic acid	$C_{12}H_{22}O_4$	HMDB0000623	289.1813	↓	↓
34	Malonic acid	$C_3H_4O_4$	HMDB0000691	163.0413	↓	↑
35	1-Methylnicotinamide	$C_7H_9N_2O+$	HMDB0000699	172.0412	↑	↓
36	Hydrocinnamic acid	$C_9H_{10}O_2$	HMDB0000764	299.1288	↓	↓
37	Propionylcarnitine	$C_{10}H_{19}NO_4$	HMDB0000824	433.2574	↓	↓
38	Neuraminic acid	$C_9H_{17}NO_8$	HMDB0000830	266.0881	↑	↓
39	Pelargonic acid	$C_9H_{18}O_2$	HMDB0000847	315.2538	↓	↓
40	Tetradecanedioic acid	$C_{14}H_{26}O_4$	HMDB0000872	257.1763	↓	↓
41	Tetrahydrocortisone	$C_{21}H_{32}O_5$	HMDB0000903	363.2167	↓	↓
42	5-Aminolevulinic acid	$C_5H_9NO_3$	HMDB0001149	261.1093	↑	↓
43	Diadenosine tetraphosphate	$C_{20}H_{28}N_{10}O_{19}P_4$	HMDB0001211	835.0386	↑	↓
44	FAD	$C_{27}H_{33}N_9O_{15}P_2$	HMDB0001248	784.1475	↓	↓
45	5-Methyltetrahydrofolic acid	$C_{20}H_{25}N_7O_6$	HMDB0001396	458.1810	↑	↓
46	5,10-Methylene-THF	$C_{20}H_{23}N_7O_6$	HMDB0001533	456.1647	↑	↓
47	Ubiquinone-1	$C_{14}H_{18}O_4$	HMDB0002012	249.1135	↑	↓
48	Oleanolic acid	$C_{30}H_{48}O_3$	HMDB0002364	455.3517	↓	↑
49	Androsterone glucuronide	$C_{25}H_{38}O_8$	HMDB0002829	511.3076	↑	↓
50	Cortolone	$C_{21}H_{34}O_5$	HMDB0003128	411.2894	↑	↑
51	Retinoyl b-glucuronide	$C_{26}H_{36}O_8$	HMDB0003141	535.2716	↑	↑
52	Cortol	$C_{21}H_{36}O_5$	HMDB0003180	735.5037	↓	↑
53	5-Acetylamino-6-formylamino-3-methyluracil	$C_8H_{10}N_4O_4$	HMDB0011105	225.0621	↓	↓
54	Cyclohexanecarboxylic acid	$C_7H_{12}O_2$	HMDB0031342	255.1599	↓	↓
55	Heptanal	$C_7H_{14}O$	HMDB0031475	227.2021	↓	↓

Trend 1 indicated the changing information of differential metabolites between control and model groups; Trend 2 indicated the changing information of differential metabolites between model and BAPs-H groups.

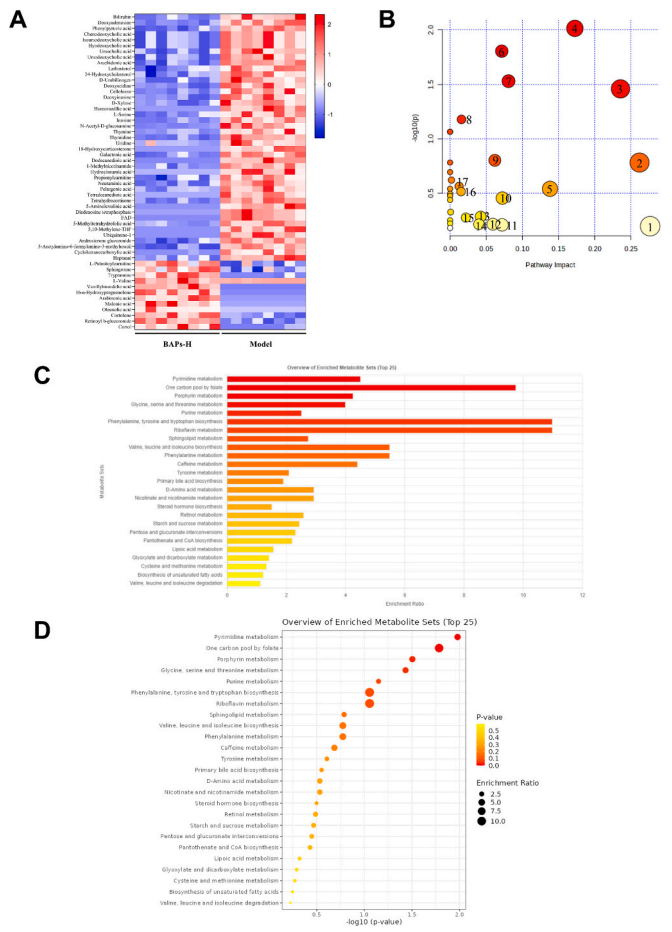

Fig. 5. Changes in metabolic profiling of fecal samples and corresponding pathway analysis (n = 8). (A) Heatmap analysis of fecal metabolites in hyperlipidemia rats treated with BAPs-H. (B) KEGG pathway analysis of fecal metabolites between model and BAPs-H groups (1, Arachidonic acid metabolism. 2, Phenylalanine metabolism. 3, Glycine, serine and threonine metabolism. 4, Pyrimidine metabolism. 5, Nicotinate and nicotinamide metabolism. 6, One carbon pool by folate. 7, Porphyrin metabolism. 8, Purine metabolism. 9, Sphingolipid metabolism. 10, Pentose and glucoronate interconversions. 11, Amino sugar and nucleotide sugar metabolism. 12, Steroid biosynthesis. 13, Glyoxylate and dicarboxylate metabolism. 14, Tryptophan metabolism. 15, Cysteine and methionine metabolism. 16, Steroid hormone biosynthesis. 17, Primary bile acid synthesis). (C—D) Metabolic pathway enrichment analysis based on fecal metabolites between model and BAPs-H groups.

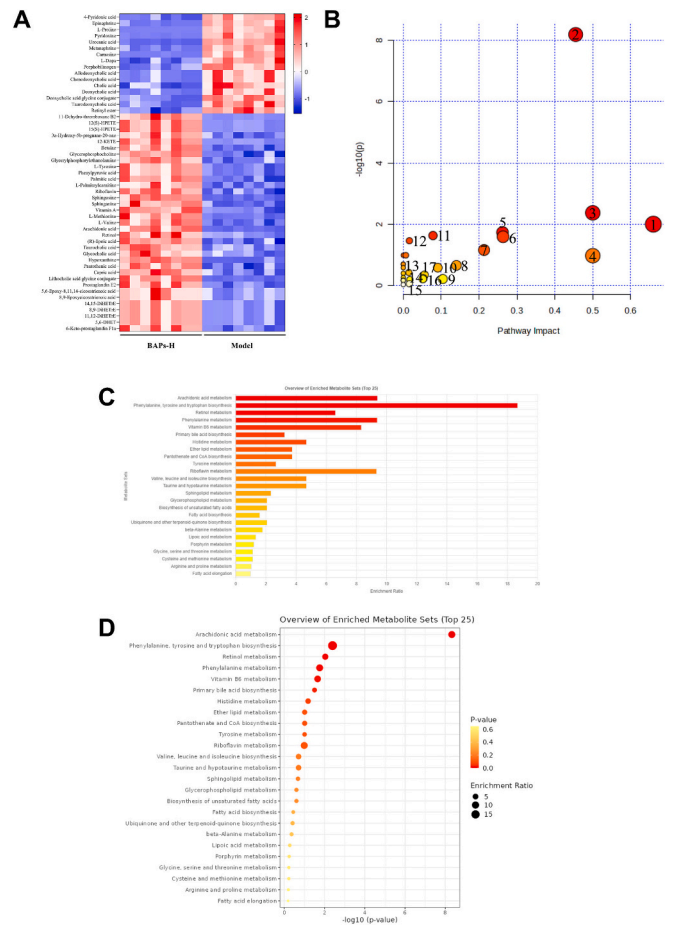

Fig. 6. Changes in metabolic profiling of liver samples and corresponding pathway analysis (n = 8). (A) Heatmap analysis of liver metabolites in hyperlipidemia rats treated with BAPs-H. (B) KEGG pathway analysis of liver metabolites between model and BAPs-H groups (1, Retinol metabolism. 2, Arachidonic acid metabolism. 3, Phenylalanine, tyrosine and tryptophan biosynthesis. 4, Riboflavin metabolism. 5, Phenylalanine metabolism. 6, Tyrosine metabolism. 7, Histidine metabolism. 8, Sphingolipid metabolism. 9, Cysteine and methionine metabolism. 10, Glycerophospholipid metabolism. 11, Vitamin B6 metabolism. 12, Primary bile acid biosynthesis. 13, Fatty acid biosynthesis. 14, Arginine and proline metabolism. 15, Purine metabolism. 16, Glycine, serine and threonine metabolism. 17, beta-Alanine metabolism). (C-D) Metabolic pathway enrichment analysis based on liver metabolites between model and BAPs-H groups.

was found that arachidonic acid metabolism, phenylalanine metabolism, sphingolipid metabolism and primary bile acid biosynthesis were the commonly enriched pathways of the two metabolomics. The findings indicated that lipid metabolism and amino acid metabolism made an important contribution in the process of ameliorating hyperlipidemia by the intervention of BAPs-H. Therefore, the crucial targets involved in the synthesis, decomposition and transport of lipids needed to be investigated to verify the objectivity of lipid metabolism-related pathways. Additionally, a study have demonstrated that phenylalanine metabolism played a crucial role in reducing blood lipids by mediating the SREBP/HMGCR signaling pathway, which interfered with cholesterol synthesis and transport [42].

3.6. *Effect of BAPs intake on improved liver lipid metabolism*

3.6.1. *Multivariate statistical analysis*

As shown in Fig. 7 A-C, PCA was used to visualize the classification of differential lipids among the groups, including the QC samples. The PCA results revealed that the QC samples from six consecutive injections clustered tightly together, demonstrating that both the lipid extraction process and the instrument detection had high repeatability. This confirmed that the stability of the instrument was excellent, ensuring reliable data for further analysis. Moreover, the lipid profiling of the control, model, and BAPs-H groups exhibited significant separation, indicating that the HFD significantly altered the lipid profile in rat liver. However, treatment with BAPs-H resulted in a marked reversal of these lipid metabolism changes, bringing the lipid profile closer to that of the control group. To further assess lipid differences, a supervised OPLS-DA model was applied (Fig. 7D). The validation parameters for this model were as follows: $R^2Y = 0.998$, $Q^2 = 0.934$, indicating excellent model fitness and predictability. The results of the permutation test showed $R^2 = 0.975$, $Q^2 = -0.158$, suggesting that the OPLS-DA model was reliable and capable of predicting changes in lipid profiling (Fig. 7E). The OPLS-DA score plot showed clear separation between the model and BAPs-H groups, further confirming that BAPs-H significantly improved the disrupted lipid metabolism. S-plot analysis based on the OPLS-DA model (Fig. 7F) provided the VIP values for differential lipids. The red dots on the plot indicate lipids with VIP values >1, suggesting that these lipids

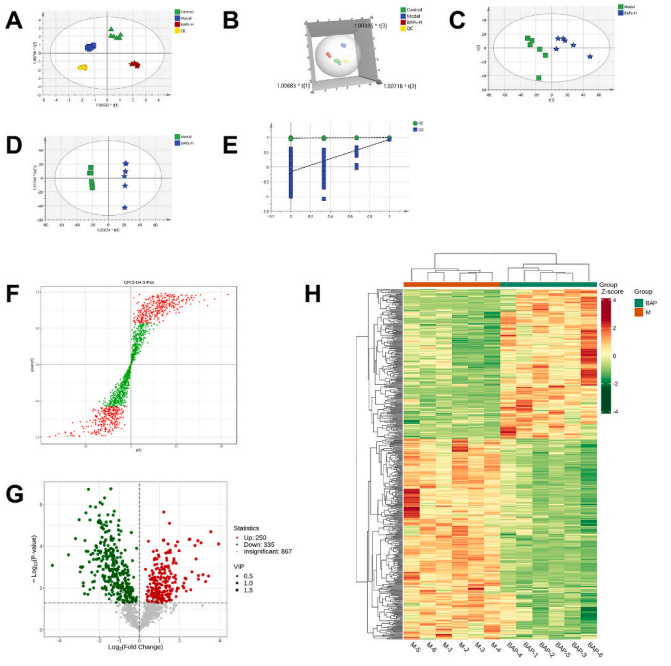

Fig. 7. Multivariate statistical analysis of liver lipid-metabolic profiles before and after BAPs-H treatment (liver tissues, $n = 6$). (A) PCA score plot for the control, model, BAPs-H, and QC groups (2D). (B) PCA score plot for the control, model, BAPs-H, and QC groups (3D). (C) PCA score plot for the model and BAPs-H groups (2D). (D) OPLS-DA score plot for the model and BAPs-H groups. (E) Permutation test for established OPLS-DA model. (F) S-plot score for the model and BAPs-H groups. (G) Volcano map analysis of differential lipids between model and BAPs-H groups. (H) Heat-map analysis of identified differential lipids.

exhibit significant differences between the groups and can be considered as potential lipid biomarkers. Additionally, volcano plot analysis (Fig. 7G) visually depicted the relative lipid content differences between the groups, serving as an effective tool to identify differential lipids.

3.6.2. *Identification of differential lipids in rat liver*

Following the established literature, we applied the screening criteria of $P < 0.05$, VIP > 1, and FC ≥ 2 or ≤ 0.5 to identify potential lipid biomarkers. Through volcano plot and heat-map analysis (Fig. 7G-H), a total of 1452 differential lipids were identified among the control, model, and BAPs-H groups. However, 867 of these lipids showed no significant differences, suggesting that they were not suitable as biomarkers for the lipid-lowering effect of BAPs-H. Treatment with BAPs-H notably increased the expression of 250 lipids while downregulating 335 lipids. These lipids were categorized into four major lipid groups and 16 lipid subclasses, including lysophosphatidylcholines (LysoPCs), lysophosphatidic acids (LysoPAs), lysophosphatidylethanolamines (LysoPEs), lysophosphatidylglycerols (LysoPGs), lysophosphatidylinositols (LysoPIs), lysophosphatidylserines (LysoPSs), phosphatidic acid (PA), phosphatidylcholines (PC), phosphatidylethanolamines (PE), phosphatidylinositols (PI), phosphatidylglycerols (PG), phosphatidylserines (PS), ceramides (Cer), diacylglycerols (DG), TG, carnitine, and free fatty acids (FFA). Among these lipids, glycerophospholipids made up the largest proportion (63.59 %), followed by sphingolipids (15.56 %), glycerolipids (13.33 %), and fatty acyls (5.64 %). Notably, BAPs-H supplementation significantly reversed the levels of 66 lipids (Table 7), effectively improving hyperlipidemia through the regulation of these biomarkers. Specifically, BAPs-H supplementation increased the expression levels of 20 lipids and decreased the expression of 46 lipids in HFD-induced hyperlipidemia rats.

Table 7
The significantly reversed lipid biomarkers among control, model and BAPs-H groups.

No.	Compound ID	Formula	*P*-value	VIP	Trend 1	Trend 2
1	LPG(18:1/0:0)	$C_{24}H_{47}O_9P$	6.49E-03	1.30	↑	↓
2	LPI(16:0/0:0)	$C_{25}H_{49}O_{12}P$	2.34E-02	1.19	↓	↑
3	PE(16:0_16:0)	$C_{37}H_{74}NO_8P$	5.69E-03	1.49	↓	↑
4	PE(24:0_18:1)	$C_{47}H_{92}NO_8P$	4.11E-03	1.30	↓	↑
5	PE(18:1_18:2)	$C_{41}H_{76}NO_8P$	1.08E-02	1.18	↑	↓
6	PE(18:1_20:3)	$C_{43}H_{78}NO_8P$	3.65E-05	1.68	↑	↓
7	PE(22:6_18:2)	$C_{45}H_{74}NO_8P$	3.54E-02	1.03	↓	↑
8	PG(16:0_20:4)	$C_{42}H_{75}O_{10}P$	9.69E-03	1.48	↓	↑
9	PG(18:1_22:5)	$C_{46}H_{79}O_{10}P$	1.96E-02	1.17	↑	↓
10	PI(18:1_18:2)	$C_{45}H_{81}O_{13}P$	4.21E-05	1.53	↑	↓
11	PS(18:0_20:3)	$C_{44}H_{80}NO_{10}P$	4.23E-05	1.68	↑	↓
12	PS(18:0_20:4)	$C_{44}H_{78}NO_{10}P$	1.86E-07	1.60	↑	↓
13	LPA(0:0/16:0)	$C_{19}H_{39}O_7P$	2.57E-04	1.66	↓	↑
14	LPA(0:0/18:1)	$C_{21}H_{41}O_7P$	1.56E-04	1.46	↑	↓
15	LPA(0:0/18:2)	$C_{21}H_{39}O_7P$	2.96E-03	1.41	↑	↓
16	LNAPE(22:6/N-20:4)	$C_{47}H_{74}NO_8P$	1.38E-02	1.37	↓	↑
17	LNAPE(18:1/N-18:2)	$C_{41}H_{76}NO_8P$	1.80E-02	1.11	↑	↓
18	PG(22:0_18:1)	$C_{46}H_{89}O_{10}P$	1.30E-03	1.37	↑	↓
19	PG(16:0_20:2)	$C_{42}H_{79}O_{10}P$	2.26E-02	1.16	↑	↓
20	PG(18:2_22:2)	$C_{46}H_{83}O_{10}P$	6.37E-03	1.25	↑	↓
21	PG(22:6_22:6)	$C_{50}H_{75}O_{10}P$	3.76E-02	1.37	↓	↑
22	PS(18:0_21:1)	$C_{45}H_{86}NO_{10}P$	4.41E-03	1.25	↑	↓
23	PS(18:1_21:2)	$C_{45}H_{82}NO_{10}P$	1.91E-03	1.33	↑	↓
24	PS(20:0_22:4)	$C_{48}H_{86}NO_{10}P$	8.29E-03	1.29	↑	↓
25	PS(18:1_20:4)	$C_{44}H_{84}NO_{10}P$	1.53E-03	1.36	↑	↓
26	PS(18:2_20:3)	$C_{44}H_{84}NO_{10}P$	1.77E-03	1.30	↑	↓
27	PI(18:1_20:3)	$C_{47}H_{83}O_{13}P$	3.01E-04	1.51	↑	↓
28	PI(18:1_20:4)	$C_{47}H_{81}O_{13}P$	1.76E-07	1.65	↑	↓
29	PA(20:2_22:5)	$C_{45}H_{75}O_8P$	1.83E-03	1.39	↑	↓
30	PA(20:4_22:5)	$C_{45}H_{71}O_8P$	1.19E-02	1.48	↓	↑
31	Carnitine C16:0	$C_{23}H_{45}NO_4$	1.50E-03	1.56	↓	↑
32	Carnitine C20:0	$C_{27}H_{53}NO_4$	5.39E-03	1.27	↑	↓
33	Carnitine C18-OH	$C_{25}H_{49}NO_5$	1.01E-02	1.39	↓	↑
34	Cer(d18:1/19:0)	$C_{37}H_{73}NO_3$	3.93E-02	1.09	↓	↑
35	LPC(14:0/0:0)	$C_{22}H_{46}NO_7P$	3.34E-03	1.45	↓	↑
36	LPC(0:0/15:0)	$C_{23}H_{48}NO_7P$	1.83E-03	1.58	↓	↑
37	LPC(16:0/0:0)	$C_{24}H_{50}NO_7P$	2.06E-04	1.71	↓	↑
38	LPC(0:0/19:0)	$C_{27}H_{56}NO_7P$	3.72E-02	1.01	↓	↑
39	LPC(0:0/18:1)	$C_{26}H_{52}NO_7P$	2.06E-04	1.42	↑	↓
40	LPC(0:0/20:1)	$C_{28}H_{56}NO_7P$	1.01E-02	1.43	↑	↓
41	LPC(0:0/22:1)	$C_{30}H_{60}NO_7P$	1.97E-02	1.43	↑	↓
42	LPC(0:0/18:2)	$C_{26}H_{50}NO_7P$	2.18E-03	1.28	↑	↓
43	LPC(18:2/0:0)	$C_{26}H_{50}NO_7P$	1.15E-03	1.29	↑	↓
44	LPC(0:0/20:2)	$C_{28}H_{54}NO_7P$	5.54E-03	1.61	↑	↓
45	LPC(20:3/0:0)	$C_{28}H_{52}NO_7P$	2.04E-04	1.56	↑	↓
46	LPC(0:0/22:4)	$C_{30}H_{54}NO_7P$	1.74E-03	1.55	↑	↓
47	LPC(22:4/0:0)	$C_{30}H_{54}NO_7P$	2.38E-03	1.53	↑	↓
48	LPE(0:0/20:3)	$C_{25}H_{46}NO_7P$	4.71E-02	1.07	↑	↓
49	PC(18:0_22:4)	$C_{48}H_{88}NO_8P$	2.72E-03	1.62	↑	↓
50	PC(O-20:1_20:4)	$C_{48}H_{88}NO_7P$	9.54E-04	1.46	↑	↓
51	PE(P-16:0_22:6)	$C_{43}H_{74}NO_7P$	4.43E-03	1.38	↓	↑
52	PE(P-18:1_22:6)	$C_{45}H_{76}NO_7P$	6.77E-03	1.41	↓	↑
53	SM(d18:1/19:0)	$C_{42}H_{85}N_2O_6P$	1.24E-03	1.45	↓	↑
54	SM(d18:1/22:1)	$C_{45}H_{89}N_2O_6P$	1.08E-02	1.18	↑	↓
55	SM(d18:1/23:1)	$C_{46}H_{91}N_2O_6P$	2.37E-02	1.21	↓	↑
56	Cer(t30:0/18:1(2OH))	$C_{48}H_{95}NO_5$	2.19E-03	1.43	↑	↓
57	Cer(d16:0/18:1)	$C_{34}H_{67}NO_3$	7.09E-04	1.62	↑	↓

(*continued on next page*)

Table 7 (*continued*)

No.	Compound ID	Formula	*P*-value	VIP	Trend 1	Trend 2
58	Cer(d18:1/15:0)	$C_{33}H_{65}NO_3$	1.43E-02	1.39	↑	↓
59	Cer(d18:1/23:1)	$C_{41}H_{79}NO_3$	3.70E-04	1.52	↑	↓
60	Cer(d18:1/25:1)	$C_{43}H_{83}NO_3$	6.32E-03	1.25	↑	↓
61	Cer(d18:2/19:0)	$C_{37}H_{71}NO_3$	9.31E-05	1.63	↑	↓
62	Cer(d18:2/24:2)	$C_{42}H_{77}NO_3$	1.75E-04	1.51	↑	↓
63	Cer(d18:2/25:1)	$C_{43}H_{81}NO_3$	1.24E-02	1.09	↑	↓
64	HexCer(d18:1/23:1)	$C_{47}H_{89}NO_8$	1.47E-03	1.50	↑	↓
65	Cer(d18:2/22:0(2OH))	$C_{40}H_{77}NO_4$	6.52E-03	1.38	↑	↓
66	Cer(d18:2/40:1(2OH))	$C_{58}H_{111}NO_4$	1.62E-02	1.16	↑	↓

Trend 1 indicated the changing information of differential metabolites between control and model groups; Trend 2 indicated the changing information of differential metabolites between model and BAPs-H groups.

3.6.3. Metabolic pathway enrichment analysis

To explore the metabolic pathways related to lipid metabolism in hyperlipidemia rats, a KEGG pathway enrichment analysis was performed. As shown in Fig. 8, supplementation with BAPs-H significantly improved several metabolic pathways, including glycerophospholipid metabolism, Leishmaniasis, glycine, serine and threonine metabolism, linoleic acid metabolism, alpha-linoleic acid metabolism, arachidonic acid metabolism, primary bile acid biosynthesis, and glycosylphosphatidylinositol (GPI)-anchor biosynthesis, among others. After a combination analysis with KEGG pathways of liver metabolomics, it was found that glycerophospholipid metabolism, arachidonic acid metabolism and primary bile acid biosynthesis were the common pathways of hepatic metabolomics and lipidomics. Thus, the findings suggested that BAPs regulates lipid-metabolism homeostasis and cholesterol catabolism, and contributes to the amelioration of hyperlipidemia.

3.7. Regulation of BAPs ingestion on gut microbiota

Given the crucial role of gut microbiota in health maintenance and disease amelioration, we conducted metagenomics analysis of fecal samples from rats treated with high-dose BAPs, as well as from model rats on a HFD and control rats. Alpha diversity analysis: Alpha diversity,

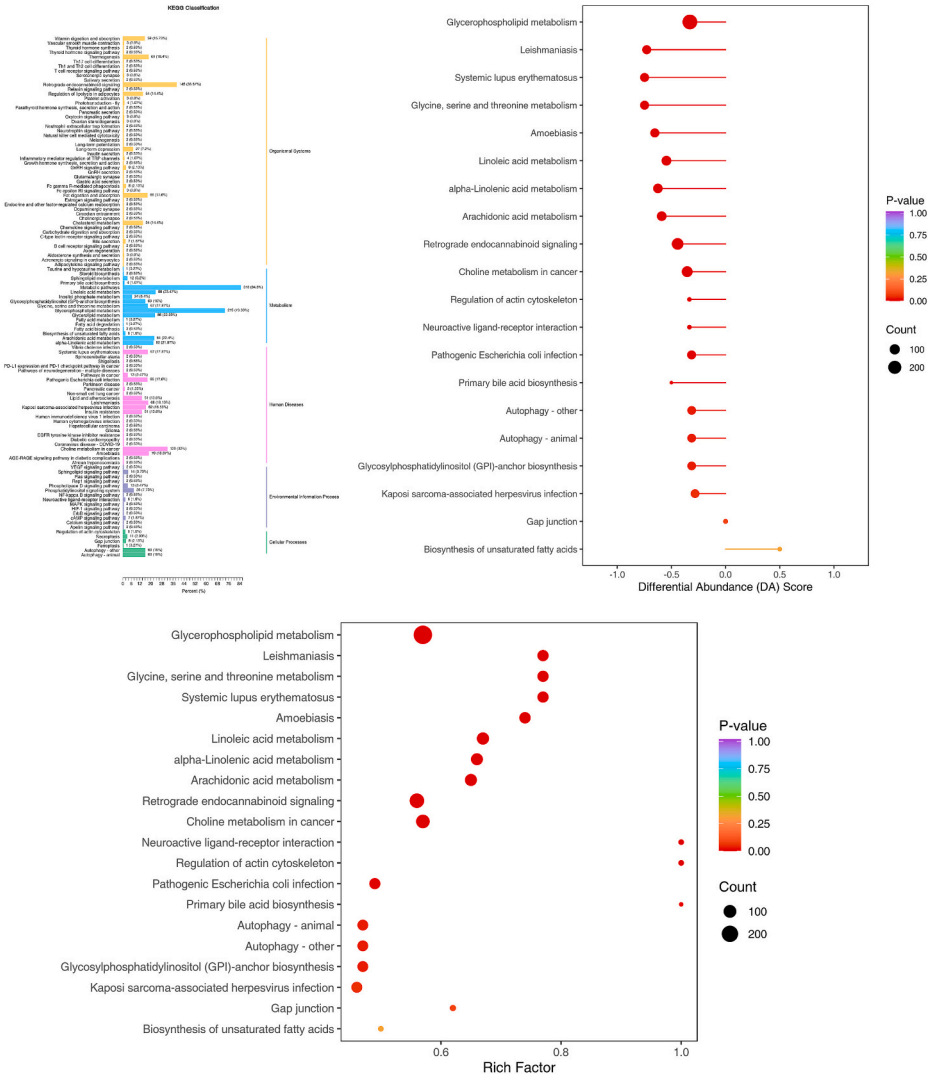

Fig. 8. Metabolic pathway of differential lipids based on the KEGG database (model vs. BAPs-H groups). Enrichment of metabolic pathways characterized by the combination of rich factor, *p*-value, and the number of differential lipids involved in the pathway.

based on ACE, Chao1, Shannon, and Simpson indices [43], showed that gut microbial richness in BAPs-H-treated rats was significantly higher than in model rats (Fig. 9A, $P < 0.05$, $P < 0.01$). This suggests that BAPs-H supplementation beneficially restored the richness of the gut microbiota in hyperlipidemia rats. Beta diversity analysis: Beta diversity analysis, including PCoA and NMDS, was performed to assess structural differences in the gut microbiota (Fig. 9B). At the species level, PCoA, PCA, and NMDS [44] results indicated that the microbiota structure changed significantly after BAPs-H treatment, with clear separation between the three groups ($P < 0.01$). These findings confirm that BAPs-H supplementation significantly altered both the abundance and the structural composition of gut microbiota.

To further examine the specific bacterial species responsible for the hypolipidemic effects of BAPs-H, we constructed histograms to visualize the gut microbiota composition at both the phylum and species levels (Fig. 9C). At the phylum level, the gut microbiota was predominantly composed of Bacteroidota, Firmicutes, and Proteobacteria, with Bacteroidota being the most dominant. In the BAPs-H group, there was a noticeable increase in the relative abundance of Firmicutes and Proteobacteria, and a decrease in the abundance of Bacteroidota. To clarify the differences between groups, we performed Linear Discriminant Analysis Effect Size (LEfSe) to identify the most influential bacterial species (Fig. 9D-E). At the species level, BAPs-H supplementation resulted in significant changes in the abundance of specific bacteria. The relative abundance of harmful bacteria, including *Prevotella copri*, *Prevotella hominis*, *Desulfovibrionaceae bacterium LT0009*, and *Lachnospiraceae bacterium*, decreased in the BAPs-H group. Conversely, beneficial bacteria, such as *Allobaculum stercoricanis*, *Prevotella* sp. *MGM2*, and *Muribaculaceae bacterium* showed increased abundance after treatment with BAPs-H. Subsequent KEGG pathway enrichment analysis revealed that the gut microbiota influenced several key metabolic pathways, including lipid metabolism, energy metabolism, carbohydrate metabolism, and amino acid metabolism. Among these pathways, lipid metabolism and amino acid metabolism are the common findings compared with the analyses of hepatic metabolomics, hepatic lipidomics and fecal metabolomics. These results demonstrated that BAPs-H might repairing the microbial barrier through remodeling intestinal flora and regulating metabolic disorders to achieve the lipid-lowering purpose.

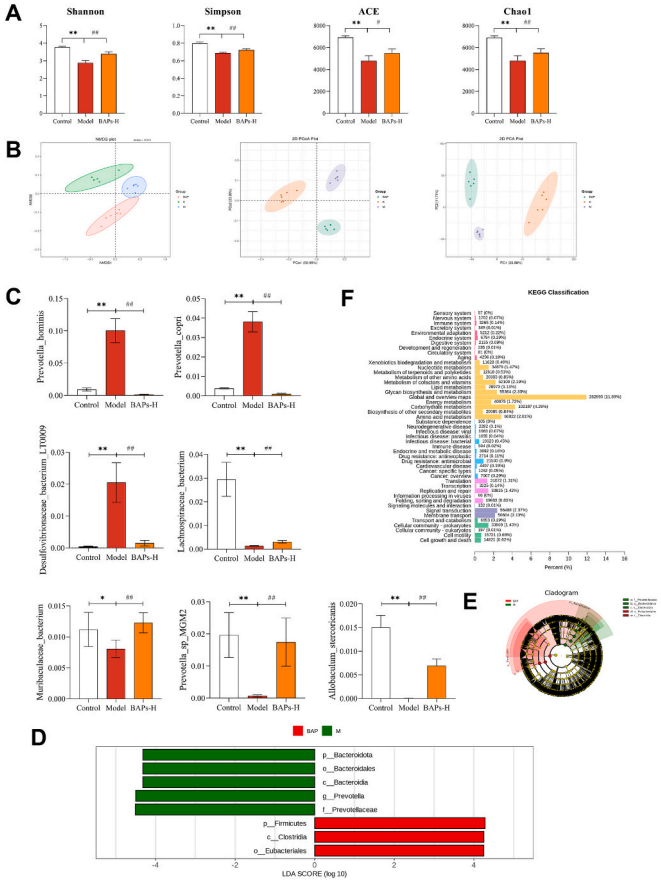

Fig. 9. Metagenomics analysis of microbiome diversity and abundance in fecal samples (fecal samples, n = 6). (A) Alpha diversity analysis (Shannon, Simpson, ACE, and Chao1 indices). (B) Beta diversity analysis (NMDS, PCoA, and PCA indices). Each point represents a sample, with points of the same color coming from the same group. (C) Comparison by the relative abundance of dominant species among the three groups. (D) Differential bacteria with LDA scores ≥4 at the phylum level across groups. (E) LEfSe analysis of phylum-level differences in gut microbiota between model and BAPs-H groups. (F) KEGG pathway enrichment analysis of microbial community functions in the model and BAPs-H groups.

3.8. Multi-omics analysis revealed that BAPs supplementation could ameliorate hyperlipidemia by modulating gut microbiota and metabolic disorders

In this section, we performed Spearman's correlation analysis to explore the potential relationships between metabolites and gut microbiota at the species level, as shown in Fig. 10. As illustrated in Fig. 10A, *Allobaculum stercoricanis*, *Prevotella* sp. *MGM2*, and *Muribaculaceae bacterium* exhibited a negative correlation with metabolites such as deoxycholic acid, arachidonic acid, 4-pyridoxic acid, L-Tyrosine, chenodeoxycholic acid, 12-KETE, 12(*S*)-HPETE, and 15(*S*)-HPETE. In contrast, they showed a positive correlation with glycerylphosphorylethanolamine, prostaglandin E2, L-Proline, and glycerophosphocholine. On the other hand, *Prevotella copri*, *Prevotella hominis*, *Desulfovibrionaceae bacterium LT0009*, and *Lachnospiraceae bacterium* displayed a positive correlation with arachidonic acid, 4-pyridoxic acid, epinephrine, 12-KETE, 12(*S*)-HPETE, 15(*S*)-HPETE, L-Methionine, L-Valine, and sphingosine, while showing a negative correlation with prostaglandin E2, L-Palmitoylcarnitine, L-Proline, and betaine. A significant correlation between bacterial species and hepatic lipids was observed through Spearman analysis, as shown in Fig. 10B. *Allobaculum stercoricanis*, *Prevotella* sp. *MGM2*, and *Muribaculaceae bacterium* were positively correlated with PG(22:6_22:6), LPC(0:0/15:0), LPA(0:0/16:0), and LPA(16:0/0:0), but negatively correlated with PI(18:1_20:3), Cer(d18:1/15:0), PE(18:1_20:3), Cer(d18:2/19:0), LPA(0:0/18:2), Carnitine C20:0, LPC(0:0/20:2), and LPC(20:3/0:0). Meanwhile, *Lachnospiraceae bacterium*, *Prevotella copri*, *Prevotella hominis*, and *Desulfovibrionaceae bacterium LT0009* showed a negative correlation with PE(P-16:0_22:6), PE(P-18:1_22:6), LPA(0:0/16:0), LPC(16:0/0:0), SM (d18:1/19:0), while being positively correlated with PG(22:0/18:1), PC (18:0/22:4), Cer(d18:1/23:1), Cer(d18:2/25:1), PS(18:0/20:3), PA (20:2/22:5), and others. As shown in Fig. 10C, *Lachnospiraceae bacterium*, *Allobaculum stercoricanis*, and *Prevotella* sp. *MGM2* were significantly and positively correlated with cortol, vanillylmandelic acid, 16-a-hydroxypregnenolone, and tryptamine, but negatively correlated with neuraminic acid, FAD, tetradecanedioic acid, cyclohexanecarboxylic acid, ubiquinone-1, dodecanedioic acid, hydrocinnamic acid, diadenosine tetraphosphate, 1-methylnicotinamide, and D-xylose. Conversely, the relative abundance of *Desulfovibrionaceae bacterium LT0009*, *Prevotella copri*, and *Prevotella hominis* showed a negative correlation with malonic acid, cortol, vanillylmandelic acid, and 16-a-hydroxypregnenolone, while positively correlating with ubiquinone-1, dodecanedioic acid, hydrocinnamic acid, diadenosine tetraphosphate, homovanillic acid, and galactonic acid. We further analyzed the correlation between the gut microbiota, hepatic metabolites, lipids, and phenotypic indicators. As depicted in Fig. 10D, the levels of TG, TC, AST, LDL-C, and ALT were positively correlated with cholic acid, 12-KETE, 12 (*S*)-HPETE, 15(*S*)-HPETE, L-Methionine, L-Valine, L-Tyrosine, arachidonic acid, and deoxycholic acid, while negatively correlated with (*R*)-lipoic acid, phenylpyruvic acid, L-Proline, and L-Palmitoylcarnitine.

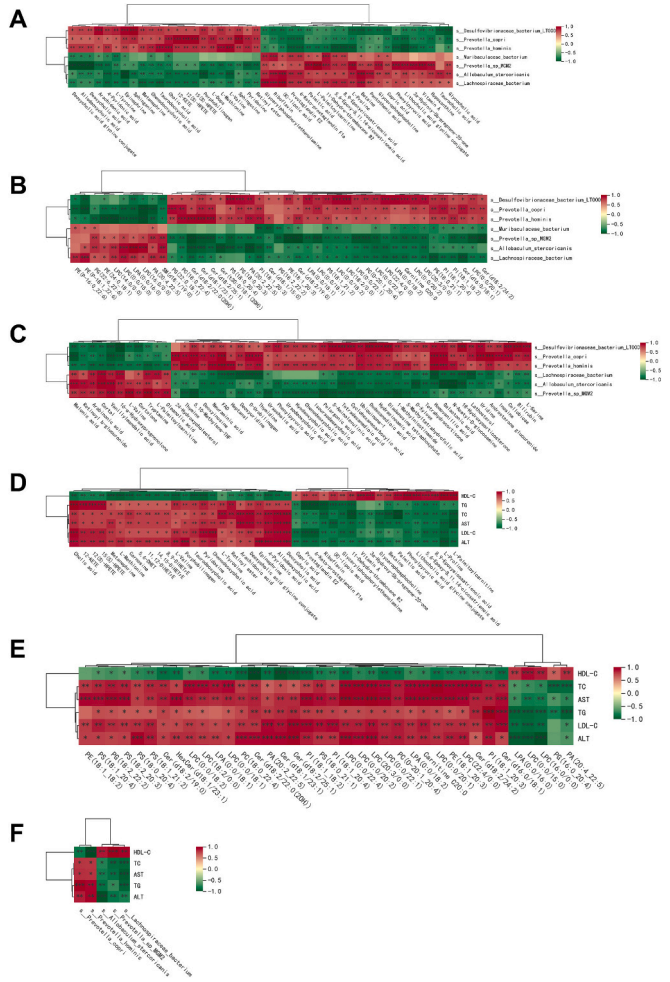

Fig. 10. Effects of BAPs-H intervention on the gut-liver axis in high-fat diet-induced hyperlipidemia rats. (A) Heatmap of Spearman correlation analysis between the crucial gut microbial taxa and hepatic metabolites. (B) Heatmap of Spearman correlation analysis between the crucial gut microbial taxa and hepatic lipids. (C) Heatmap of Spearman correlation analysis between the crucial gut microbial taxa and fecal metabolites. (D) Spearman correlation between hepatic metabolome and phenotype. (E) Spearman correlation between hepatic lipids and phenotype. (F) Spearman correlation between gut microbiota and phenotype.

Additionally, Fig. 10E shows that the levels of TC, TG, AST, and ALT were significantly positively correlated with Cer(d18:2/19:0), PC(18:0/22:4), Cer(d18:2/22:0(2-OH)), Cer(d18:1/23:1), and PI(18:1/20:3), but negatively correlated with LPC(0:0/15:0), LPC(16:0/0:0), and PA(20:4/22:5). The correlation between gut microbiota and phenotypic indicators is shown in Fig. 10F. The expression levels of TC, TG, AST, and ALT were positively correlated with *Prevotella copri* and *Prevotella hominis*, while negatively correlated with *Lachnospiraceae bacterium*, *Allobaculum stercoricanis*, and *Prevotella* sp. *MGM2*. Interestingly, the correlation between HDL-C and gut microbiota was opposite to the trends observed for other phenotypic indicators. Overall, these results demonstrate that the identified metabolites, lipids, and bacterial species play crucial roles in ameliorating hyperlipidemia.

3.9. Effects of BAPs-H on the expression of genes and proteins involving in lipid metabolism in high-fat diet-induces hyperlipidemia rats

In this section, we employed ELISA, qRT-PCR, and Western blotting techniques to assess the enzyme activities and transcript levels of key regulatory factors involved in lipid metabolism (Fig. 11 and Fig. 12).

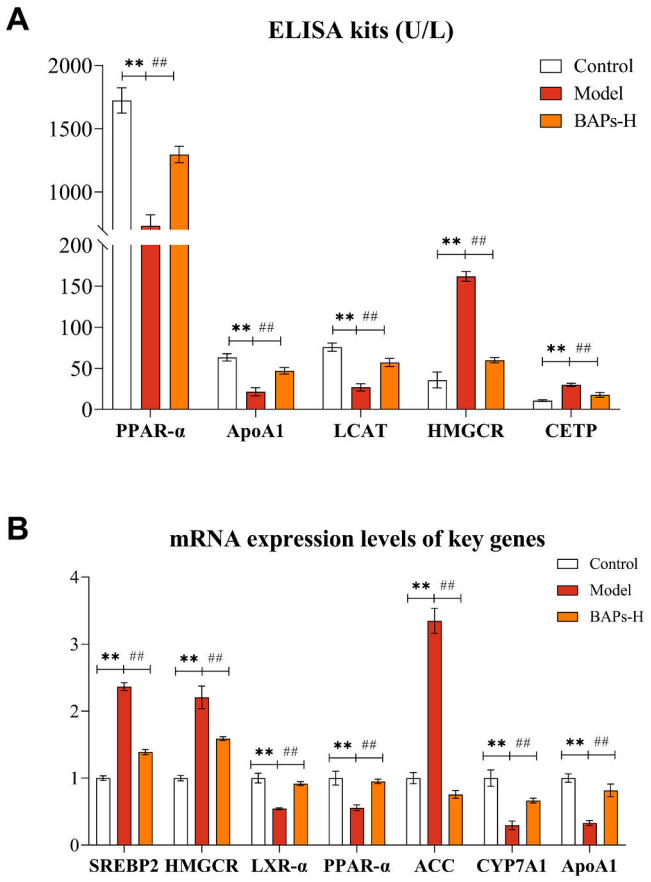

Fig. 11. Effects of BAPs-H supplementation on the protein and mRNA expression levels of crucial genes associated with lipid and cholesterol metabolism (liver tissues). (A) The expression of PPAR-α, ApoA1, LCAT, HMGCR and CETP at the protein level (n = 8). (B) The expression of SREBP2, HMGCR, LXR-α, PPAR-α, ACC, CYP7A1 and ApoA1 at the mRNA level (n = 8). Data are expressed as the mean ± SD. $^{*}P < 0.05$, $^{**}P < 0.01$, compared with the Control group; $^{\#}P < 0.05$, $^{\#\#}P < 0.01$, compared with the Model group.

Compared to the control group, the enzyme activities of HMGCR (3-hydroxy-3-methylglutaryl-CoA reductase) and CETP (cholesteryl ester transfer protein) were significantly elevated in the model group, while the activities of PPAR-α (peroxisome proliferator-activated receptor alpha), ApoA1 (apolipoprotein A1), and LCAT (lecithin-cholesterol acyltransferase) were markedly reduced (Fig. 11A, $P < 0.01$). After supplementation with BAPs-H, the enzyme activities of PPAR-α, ApoA1, and LCAT were significantly restored ($P < 0.01$), while the activities of HMGCR and CETP were significantly suppressed ($P < 0.01$). The mRNA expression levels of genes associated with lipid production, lipid transport, cholesterol biosynthesis, and cholesterol metabolism were assessed using qRT-PCR. As shown in Fig. 11B, compared to the control group, the expression levels of SREBP2, HMGCR, and ACC were significantly elevated in the model group. Conversely, the mRNA expression levels of LXR-α (liver X receptor alpha), PPAR-α, CYP7A1, and ApoA1 were markedly reduced ($P < 0.01$). After BAPs-H treatment, the expression levels of SREBP2, HMGCR, and ACC were significantly lower than those in the model group, while the expression of LXR-α, PPAR-α, CYP7A1, and ApoA1 was significantly higher ($P < 0.01$). Western blotting was performed to assess the protein levels of SREBP2, HMGCR, LXR-α, PPAR-α, CYP7A1, and PPAR-γ. As depicted in Fig. 12, the HFD led to a marked increase in the production of SREBP2 and HMGCR, along with a decrease in the expression of LXR-α, PPAR-α, CYP7A1, and PPAR-γ ($P < 0.01$). In contrast, BAPs-H supplementation significantly reversed the changes in the expression of these proteins. These results suggest that BAPs-H modulates lipid metabolism through the regulation of key

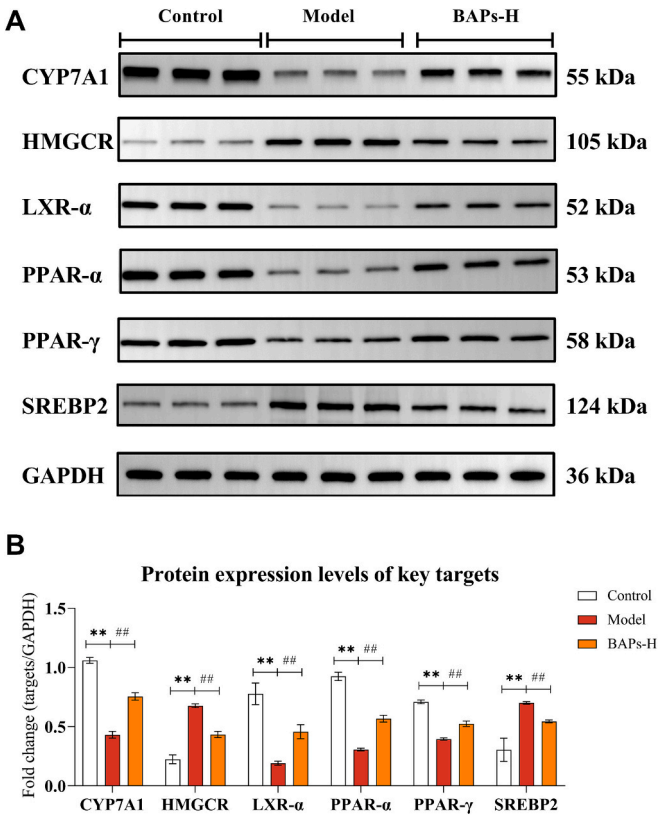

Fig. 12. Western blotting analysis was adopted to visualize and quantify the protein expression levels of crucial targets associated with lipid metabolism affected by BAPs-H in hyperlipidemia rats (liver tissues, $n = 3$). (A) Visualized analysis of western blotting data. (B) Quantitative analysis of western blotting based on gray values. Data are expressed as the mean ± SD. $^{*}P < 0.05$, $^{**}P < 0.01$, compared with the Control group; $^{\#}P < 0.05$, $^{\#\#}P < 0.01$, compared with the Model group.

transcription factors and enzymes, likely contributing to its lipid-lowering effects by inhibiting cholesterol synthesis and promoting lipid oxidation and metabolism.

4. Discussion

In a previous study conducted by our team, we demonstrated that bile *Arisaema* and its key active compound, BAP, exert significant antipyretic effects in dry yeast-induced hyperthermic rats by modulating metabolic disturbances [25]. Furthermore, we observed that BAP could restore disturbed intestinal flora to nearly normal levels under febrile conditions. Building on these findings, the current study further explores the potential mechanism by which BAPs (without free proteins) exert lipid-lowering effects through the modulation of gut microbiota and lipid metabolic disorders. We have previously shown that the aqueous extract of bile *Arisaema* possesses notable lipid-lowering properties through various animal experiments. Based on these results, we hypothesize that polysaccharides might be the key active constituents responsible for this effect. Unfortunately, due to publishing restrictions, the corresponding findings have not yet been made publicly available.

4.1. The phytochemical properties of BAPs

Extensive evidence suggests that the lipid-lowering effects of plant polysaccharides are largely dependent on their structural characteristics, such as molecular weight, chemical composition, and backbone structure [45]. To investigate the chemical properties of BAPs, we conducted a series of experiments prior to the animal studies. Notably, in this study, we made some adjustments to the preparation and purification of the BAP samples. Firstly, potential free proteins were removed from the samples using the Sevage method. Secondly, methylation analysis was performed for the first time to explore the preliminary backbone structure of BAPs, providing a foundation for the future purification and separation of monosaccharides and structural analysis. The monosaccharide composition of the BAPs prepared in this study was found to be similar to that of BAPs previously isolated from bile *Arisaema*. However, there were slight variations in the proportions of the monosaccharides, while the types of monosaccharides remained unchanged. These differences could be attributed to factors such as the high temperature employed during the decoction of bile *Arisaema* or overreaction during the acid hydrolysis process. Additionally, the application of the Sevage method led to a reduction in the total protein content, which consequently lowered the molecular weight of peak 1. A particularly noteworthy aspect of this study is the investigation of the backbone structure of BAPs using methylation analysis, which is being reported for the first time. This analysis revealed the preliminary repeating unit structure and the degree of branching, thus filling a gap in the structural analysis of polysaccharides from bile *Arisaema*. In the future, we plan to continue our investigations by isolating and purifying monomeric polysaccharides, and conducting further structural characterization through techniques such as partial acid hydrolysis, Smith degradation, and nuclear magnetic resonance (NMR) spectroscopy.

4.2. The pharmacodynamics investigation of BAPs in high-fat diet-induced hyperlipidemia rats

Rodent models of hyperlipidemia are commonly used to study human lipid-related diseases and evaluate blood lipid regulation [46]. A high-fat, high-cholesterol diet is a primary factor in inducing hyperlipidemia, and the formulation of the diet plays a crucial role in determining the success of the model. In the present study, we induced hyperlipidemia in male SD rats using a diet containing 10 % fat and 5 % cholesterol, based on preliminary experiments conducted by our team. After a four-weeks modeling, the blood lipid levels of rats have been dramatically altered, suggesting the successful inducement of hyperlipidemia. Then, high-dose BAPs supplementation exhibited unexpected effect on ameliorating hyperlipidemia and protecting liver tissue. Adipose tissue has been recognized as a critical regulator of metabolic balance across various tissues, playing an essential role in maintaining systemic metabolic homeostasis [47,48]. In this study, we demonstrated that high-dose BAP treatment significantly reduced lipid accumulation in epididymal fat induced by the HFD, indicating that BAP-H intervention might regulate lipid metabolism to lower blood lipids. This finding also provided powerful evidence for subsequent investigation.

4.3. Potential mechanism of BAPs in lowering blood lipids: regulating lipid metabolism

Lipidomics analysis has garnered increasing attention in recent years, as it allows for the precise quantification of various lipid species in liver tissues and provides detailed insights into their fatty acid composition [49,50]. In the present study, we employed untargeted metabolomics and widely targeted lipidomics to identify classical biomarkers that may contribute to the improvement of hyperlipidemia through BAPs-H administration. Additionally, molecular biological techniques were used to validate the key enzymes involved in critical metabolic pathways identified by the metabolomic and lipidomic analyses.

Our findings indicated that several metabolic pathways, including arachidonic acid metabolism, tryptophan metabolism, phenylalanine metabolism, sphingolipid metabolism, glycerophospholipid metabolism, and glycine, serine, and threonine metabolism, as well as primary bile acid biosynthesis, played significant roles in regulating metabolic disorders and ameliorating hyperlipidemia. Notably, arachidonic acid metabolism emerged as a central pathway underlying the

lipid-lowering effects of BAPs. Untargeted metabolomics and lipidomics analysis revealed a large accumulation of arachidonic acid metabolites in the liver, which is consistent with previous reports of hyperlipidemia [51]. Arachidonic acid metabolism was reported to increase hepatic lipid accumulation through regulating ACC and fatty acid synthase (FAS) [52]. Our results indicated a significant reduction in the expression levels of these metabolites following BAPs-H treatment, suggesting that BAPs inhibited arachidonic acid metabolism in hyperlipidemia rats. Sphingolipids, which are abundant in liver tissues, have been implicated in the pathogenesis of metabolic diseases, including hepatic steatosis [53]. In our study, BAPs-H supplementation led to the downregulation of sphingolipid metabolites, such as ceramide and sphingosine, in HFD-induced hyperlipidemia rats. Ceramides, in particular, are known to contribute to LDL aggregation, inflammatory responses, vascular inflammation, and the formation of atherosclerosis [54]. Furthermore, glycerophospholipids, which are the primary components of biomembranes, were also significantly affected by BAPs. Among these, LPC was found to be the most abundant in our analysis. Li et al. demonstrated that LPC plays a critical role in oxidizing LDL, promoting foam cell formation, damaging vascular endothelial cells, and activating oxidative stress and inflammation [55].

Increasing evidence suggests that the pathogenesis and progression of hyperlipidemia are closely associated with disturbances in amino acid metabolism [56]. Elevated levels of certain amino acids have been observed in individuals with obesity and dyslipidemia [57], both in children and adults. In this study, we observed that BAPs-H treatment significantly reversed the high levels of amino acids—including tyrosine, alanine, proline, methionine, phenylalanine, and valine—induced by a HFD. Mook-Kanamori et al. found that elevated proline levels were strongly correlated with an increased risk of hyperlipidemia during a 7-year follow-up [58]. Similarly, elevated tyrosine levels have been linked to higher serum cholesterol concentrations and are closely associated with insulin resistance in obesity [59]. High methionine levels, particularly in the liver, have been observed in HFD-induced hyperlipidemia rats, though these can be reversed by treatment with berberine [60]. Furthermore, increasing phenylalanine levels has been associated with cardiac dysfunction during natural aging, and reducing valine levels has been shown to restore metabolic health in diet-induced obesity models [61]. The elevated amino acid levels in HFD-induced hyperlipidemia rats observed in this study are consistent with previous reports, suggesting that these elevated amino acids contribute to the disruption of blood lipid homeostasis [62]. Importantly, our results show that BAPs-H supplementation significantly reduced the content of these amino acids in the liver, indicating that regulation of amino acid metabolism may be a crucial pathway through which BAPs ameliorate hyperlipidemia.

In light of the integrated metabolomics and lipidomics analyses, BAPs are confirmed to ameliorate hyperlipidemia by modulating pathways involved in lipid metabolism. KEGG pathway enrichment analysis of both metabolomics and lipidomics data highlighted several pathways, including the biosynthesis of unsaturated fatty acids, glycerophospholipid metabolism, arachidonic acid metabolism, and primary bile acid biosynthesis. These findings suggest that BAPs alleviate hyperlipidemia through the regulation of targets involved in lipid metabolism. Consistent with existing literature, these metabolites and lipids are known to be involved in the synthesis, breakdown, and transport of lipids and cholesterol [63]. To further elucidate the molecular mechanisms underlying BAPs' lipid-lowering effects, we employed ELISA, western blotting, and qRT-PCR techniques. It has been well-established that PPAR-α plays a key role in regulating fatty acid catabolism, ketone body synthesis, and lipogenesis [64]. Our results revealed an increase in the expression levels of PPAR-α at both the protein and mRNA levels in liver tissues following BAPs-H treatment, suggesting that BAPs promote lipid oxidation. ACC, a critical enzyme regulating lipid synthesis, is associated with increased fat production [65]. BAPs-H supplementation significantly reduced the expression of ACC mRNA, which in turn decreased the TG content. ApoA1, a carrier protein for HDL—C, plays an important role in enhancing cholesterol solubility by binding to free cholesterol, thus promoting its transport to the liver for catabolism [66]. Additionally, ApoA1 positively regulates LCAT activity, further promoting TG transport to the liver [67]. In our study, we found that a HFD led to impaired ApoA1 function, resulting in the failure to bind cholesterol and activate LCAT, leading to cholesterol accumulation. However, BAPs-H treatment significantly increased the expression levels of LCAT and ApoA1, suggesting that BAPs-H lowers blood lipid levels by promoting cholesterol transport and catabolism while inhibiting cholesterol accumulation. Cholesterol biosynthesis occurs via two main pathways: 1) regulation of SREBP processing and 2) sterol-induced degradation of HMGCR [68,69]. Our results showed that BAPs-H treatment significantly reduced the expression levels of both SREBP2 and HMGCR at the protein and mRNA levels in hyperlipidemia rats, indicating that BAPs-H inhibits cholesterol biosynthesis, contributing to its lipid-lowering effects. Additionally, CYP7A1, a crucial enzyme in cholesterol metabolism, accelerates the conversion of cholesterol to bile acids upon activation [70]. In our study, BAPs-H supplementation elevated the expression of CYP7A1, which may promote cholesterol metabolism and bile acid synthesis.

4.4. BAPs might ameliorate hyperlipidemia through modulating gut microbiota

In the current study, metagenomic analysis revealed significant changes in the gut microbiota composition in HFD-induced hyperlipidemia rats across the three experimental groups (control, model, and BAPs-H). Specifically, a marked reduction in species richness was observed in the model group, which was supplemented with a HFD. However, BAPs-H supplementation notably restored this imbalance, as evidenced by improvements in both α-diversity and β-diversity of the gut microbiota. Metagenomic sequencing further revealed that the relative abundance of *Bacteroidetes* phylum increased in the model group, while *Firmicutes* and *Proteobacteria* phyla showed a decrease. Interestingly, after BAPs-H supplementation, these phyla exhibited the opposite trends: the relative abundance of *Firmicutes* and *Proteobacteria* increased, while *Bacteroidetes* decreased. These findings are consistent with previous reports suggesting that *Firmicutes* play a key role in regulating gut homeostasis by producing metabolites that enhance the gastrointestinal barrier and mucosal immune function [71]. Additionally, *Firmicutes* are involved in modulating amino acid metabolism to reduce intestinal oxidative stress [72]. Fecal metabolomics analysis indicated that BAPs-H treatment significantly increased the content of amino acid metabolites, suggesting that BAPs-H might ameliorate intestinal oxidative stress and inflammation induced by hyperlipidemia, which aligns with findings in the literature [73]. At the species level, *Prevotella copri* has been linked to fat accumulation in pigs and is associated with increased serum metabolites related to obesity [74]. In our study, the abundance of *Prevotella copri* was significantly reduced in the gut of hyperlipidemic rats after BAPs-H supplementation, which correlated with the upregulation of genes involved in lipolysis and lipid transport and downregulation of genes associated with lipogenesis and fat accumulation. This suggests that the inhibition of *Prevotella copri* may be an effective mechanism by which BAPs-H attenuates hyperlipidemia. Furthermore, *Prevotella hominis*, a pathogenic bacterium enriched in hypothyroid patients, was found to affect the metabolism of glutamate, short-chain fatty acids, and phospholipases [75]. *Desulfovibrionaceae bacterium LT0009*, a harmful bacterium from the *Desulfovibrionaceae* family, has been implicated in liver cancer induced by a high-fat, high-cholesterol diet. This bacterium shows phased growth during liver cancer development, a pattern also observed in hypercholesterolemia patients [76]. Metagenomic analysis revealed that the abundance of these three harmful bacteria was significantly increased in the HFD group, but BAPs-H supplementation markedly inhibited their growth. This suggests that BAPs-H may help mitigate the harmful effects caused by these pathogenic bacteria. On the other hand, *Lachnospiraceae bacterium* is

considered a potentially beneficial microbe that may mediate the effect of adiposity on insulin resistance [77]. *Allobaculum stercoricanis*, another beneficial bacterium, has been implicated in various biological processes closely associated with lipid metabolism, intestinal inflammation, and neurological diseases [78]. Particularly, *Allobaculum stercoricanis* has been shown to play a protective role against hepatic lipid accumulation under metabolic stress [79]. Experimental evidence also indicates that *Theabrownin* could promote the proliferation of *Prevotella* sp. *MGM2*, thereby alleviating metabolic syndrome induced by high-fat, high-sugar, and high-salt diets [80]. Furthermore, *Muribaculaceae bacterium*, regarded as a beneficial bacterium, has been shown to have a negative correlation with liver injury markers and inflammation in non-alcoholic steatohepatitis (NASH) mice [81]. In our study, high-dose BAP supplementation significantly enhanced the relative abundance of these four beneficial bacteria in HFD-induced hyperlipidemia rats, suggesting that promoting the growth of probiotics may be an effective strategy for BAPs to ameliorate hyperlipidemia.

4.5. The innovations and limitations of this study

Collectively, this study represents the first comprehensive investigation into the lipid-lowering potential of polysaccharide components (free from proteins) derived from *Bile Arisaema*. Using a combination of multi-omics technologies and molecular biological approaches, we demonstrated that this polysaccharide can effectively treat hyperlipidemia through multiple pathways and targets. The observed hepatoprotective effects, as well as its regulation of liver lipid metabolism and intestinal microbiota, underscore the broad therapeutic potential of BAPs. These findings suggest that BAPs could be further developed and applied as a treatment for hyperlipidemia, and future research should focus on exploring its clinical efficacy. However, several limitations of the current study should be addressed in future investigations. First, although the homogeneous polysaccharide from *Bile Arisaema* has been identified, further isolation and purification processes are required. Additionally, the fine structural characterization and detailed elucidation of the underlying lipid-lowering mechanisms remain to be explored. Second, the use of additional animal models and in vitro experiments is necessary to validate the reproducibility of the pharmacodynamics findings, which will be crucial for advancing BAPs as a potential hypolipidemic agent. Lastly, while the beneficial effects of BAPs on gut microbiota were preliminarily observed, this aspect was not fully explored in the current study. For example, the relationship between gut microbiota and bile acid metabolism was not investigated. In future work, we plan to conduct targeted bacterial/metabolite gavage and fecal microbiota transplantation experiments to further explore how BAPs modulate gut microbiota to exert its lipid-lowering effects in HFD-induced animal models.

5. Conclusion

In conclusion, BAPs were successfully extracted from *Bile Arisaema* using hot water extraction and alcohol precipitation. Structural analysis revealed that glucose was the predominant monosaccharide, with the main glycosidic linkages identified as 1,4-α-Glcp and T-α-Glcp. Moreover, BAPs demonstrated a significant lipid-lowering effect in SD rats with HFD-induced hyperlipidemia. This effect was associated with the regulation of liver-intestinal metabolic disorders and modulation of gut microbiota. Our findings not only validate the lipid-lowering pharmacological potential of BAPs but also contribute to the further development and clinical application of *Bile Arisaema* in the treatment of hyperlipidemia.

CRediT authorship contribution statement

Fa-zhi Su: Writing – original draft, Methodology, Investigation, Conceptualization. **Chen-xi Bai:** Validation, Methodology. **Wen-sen Zhang:** Methodology, Data curation. **Meng Liu:** Methodology, Data curation. **Biao Li:** Validation. **Ming-hao Sun:** Validation. **Yu-jia He:** Validation. **Yuan-ning Zeng:** Supervision. **Yan-ping Sun:** Supervision. **Bing-you Yang:** Supervision. **Hai-xue Kuang:** Writing – review & editing, Funding acquisition, Conceptualization. **Qiu-hong Wang:** Writing – review & editing, Funding acquisition, Conceptualization.

Declaration of competing interest

All authors declare no conflicts of interest.

Acknowledgements

This work was financially supported by the National Key Research and Development Program of China (2018YFC1707100); Chief Scientist of Qi-Huang Project of National Traditional Chinese Medicine Inheritance and Innovation “One Hundred Million” Talent Project (2021); Heilongjiang Touyan Innovation Team Program (2019-5-39); National Famous Old Traditional Chinese Medicine Experts Inheritance Studio Construction Program of National Administration of TCM (2022-75); The Seventh Batch of National Famous Old Traditional Chinese Medicine Experts Experience Heritage Construction Program of National Administration of TCM (2022-76); Guangdong Basic and Applied Basic Research Foundation (2023A1515110740).

Appendix A. Supplementary data

Supplementary data to this article can be found online at https://doi.org/10.1016/j.ijbiomac.2025.143932.

Data availability

Data will be available online on request.

References

[1] G. Fahed, L. Aoun, M. Bou Zerdan, S. Allam, M. Bou Zerdan, Y. Bouferraa, H.I. Assi, Metabolic syndrome: updates on pathophysiology and management in 2021, Int. J. Mol. Sci. 23 (2) (2022) 786, https://doi.org/10.3390/ijms23020786.
[2] A. Ghafouri, M.D. Estêvão, P. Alibakhshi, A.B. Pizarro, A.F. Kashani, E. Persad, H. Heydari, M. Hasani, J. Heshmati, M. Morvaridzadeh, Sumac fruit supplementation improve glycemic parameters in patients with metabolic syndrome and related disorders: a systematic review and meta-analysis, Phytomedicine 90 (2021) 153661, https://doi.org/10.1016/j.phymed.2021.153661.
[3] E. Bonora, The metabolic syndrome and cardiovascular disease, Ann. Med. 38 (1) (2006) 64–80, https://doi.org/10.1080/07853890500401234.
[4] G. Jia, J.R. Sowers, Targeting endothelial exosomes for the prevention of cardiovascular disease, Biochim. Biophys. Acta Mol. basis Dis. 1866 (8) (2020) 165833, https://doi.org/10.1016/j.bbadis.2020.165833.
[5] F. Huang, X. Zheng, X. Ma, R. Jiang, W. Zhou, S. Zhou, Y. Zhang, S. Lei, S. Wang, J. Kuang, et al., Theabrownin from Pu-erh tea attenuates hypercholesterolemia via modulation of gut microbiota and bile acid metabolism, Nat. Commun. 10 (1) (2019) 4971, https://doi.org/10.1038/s41467-019-12896-x.
[6] X. Xu, Z. Song, B. Mao, G. Xu, Apolipoprotein A1-related proteins and reverse cholesterol transport in antiatherosclerosis therapy: recent progress and future perspectives, Cardiovasc. Ther. 2022 (2022) 4610834, https://doi.org/10.1155/2022/4610834.
[7] N. Imai, D.E. Cohen, Trimming the fat: acetyl-CoA carboxylase inhibition for the management of NAFLD, Hepatology 68 (6) (2018) 2062–2065, https://doi.org/10.1002/hep.30206.
[8] N. Hu, C. Chen, J. Wang, J. Huang, D. Yao, C. Li, Atorvastatin Ester regulates lipid metabolism in hyperlipidemia rats via the PPAR-signaling pathway and HMGCR expression in the liver, Int. J. Mol. Sci. 22 (20) (2021) 11107, https://doi.org/10.3390/ijms222011107.
[9] E. Rodrigo, D. González-Lamuño, J.C. Ruiz, G. Fernández-Fresnedo, D. Isla, J. González-Cotorruelo, J.A. Zubimendi, A.L. De Francisco, M. García-Fuentes, M. Arias, Apolipoprotein C-III and E polymorphisms and cardiovascular syndrome, hyperlipidemia, and insulin resistance in renal transplantation, Am. J. Transplant. 2 (4) (2002) 343–348, https://doi.org/10.1034/j.1600-6143.2002.20409.x.
[10] X. Jia, W. Xu, L. Zhang, X. Li, R. Wang, S. Wu, Impact of gut microbiota and microbiota-related metabolites on hyperlipidemia, Front. Cell. Infect. Microbiol. 11 (2021) 634780, https://doi.org/10.3389/fcimb.2021.634780.
[11] E.J. Benjamin, S.S. Virani, C.W. Callaway, A.M. Chamberlain, A.R. Chang, S. Cheng, S.E. Chiuve, M. Cushman, F.N. Delling, R. Deo, et al., Heart disease and

stroke Statistics-2018 update: a report from the American Heart Association, Circulation 137 (12) (2018) e67–e492, https://doi.org/10.1161/CIR.0000000000000558.
[12] A.L. Komaroff, The microbiome and risk for atherosclerosis, JAMA 319 (23) (2018) 2381–2382, https://doi.org/10.1001/jama.2018.5240.
[13] E. Bender, Could a bacteria-stuffed pill cure autoimmune diseases? Nature 577 (7792) (2020) S12–S13, https://doi.org/10.1038/d41586-020-00197-z.
[14] M.W. Rohr, C.A. Narasimhulu, T.A. Rudeski-Rohr, S. Parthasarathy, Negative effects of a high-fat diet on intestinal permeability: a review, Adv. Nutr. 11 (1) (2020) 77–91, https://doi.org/10.1093/advances/nmz061.
[15] J.J. Chen, J. Xie, B.H. Zeng, W.W. Li, S.J. Bai, C. Zhou, W. Chen, H. Wei, P. Xie, Absence of gut microbiota affects lipid metabolism in the prefrontal cortex of mice, Neurol. Res. 41 (12) (2019) 1104–1112, https://doi.org/10.1080/01616412.2019.1675021.
[16] F.R. Pinu, D.J. Beale, A.M. Paten, K. Kouremenos, S. Swarup, H.J. Schirra, D. Wishart, Systems biology and multi-omics integration: viewpoints from the metabolomics research community, Metabolites 9 (4) (2019) 76, https://doi.org/10.3390/metabo9040076.
[17] P. Kreitmaier, G. Katsoula, E. Zeggini, Insights from multi-omics integration in complex disease primary tissues, Trends Genet. 39 (1) (2023) 46–58, https://doi.org/10.1016/j.tig.2022.08.005.
[18] J.H. Zhang, Study on the Interaction and Mechanism of Bioactive Compounds in *Chansu* in the Treatment of Liver Cancer Based on Multi-omics Strategy [D], Zhejiang University, 2021, https://doi.org/10.27461/d.cnki.gzjdx.2021.001966.
[19] Z.M. Jiang, S.L. Zeng, T.Q. Huang, Y. Lin, F.F. Wang, X.J. Gao, J. Li, P. Li, E.H. Liu, Sinomenine ameliorates rheumatoid arthritis by modulating tryptophan metabolism and activating aryl hydrocarbon receptor via gut microbiota regulation, Sci Bull (Beijing). 68 (14) (2023) 1540–1555, https://doi.org/10.1016/j.scib.2023.06.027.
[20] S.L. Zeng, S.Z. Li, P.T. Xiao, Y.Y. Cai, C. Chu, B.Z. Chen, P. Li, J. Li, E.H. Liu, Citrus polymethoxyflavones attenuate metabolic syndrome by regulating gut microbiome and amino acid metabolism, Sci. Adv. 6 (1) (2020) eaax6208, https://doi.org/10.1126/sciadv.aax6208.
[21] J. Wu, Y. Qiao, W. Jin, F. Jia, Z. Wang, L. Li, F. Cheng, W. Zhao, Y. Cheng, L. Zhao, Y. Li, S. Yun, J. Cao, C. Feng, Metabolomics and 16S rDNA sequencing of intestinal flora reveal the regulation of Sparassis latifolia polysaccharides on splenic immune function in lead-exposed mice, Int. J. Biol. Macromol. 280 (Pt 4) (2024) 136084, https://doi.org/10.1016/j.ijbiomac.2024.136084.
[22] H. Zhang, H. Li, B. Pan, S. Zhang, X. Su, W. Sun, T. Zhang, Z. Zhang, S. Lv, H. Cui, Integrated 16S rRNA sequencing and untargeted metabolomics analysis to reveal the protective mechanisms of polygonatum sibiricum polysaccharide on type 2 diabetes mellitus model rats, Curr. Drug Metab. 24 (4) (2023) 270–282, https://doi.org/10.2174/1389200224666230406114012.
[23] Q. Bi, W. Gu, F. Meng, X. Yang, L. Zeng, L. Liang, M. Yang, T. Zhang, J. Yu, Pharmacological and metagenomics evidence of polysaccharide from *Polygonum multiflorum* in the alleviation of insulin resistance, Int. J. Biol. Macromol. 164 (1) (2020) 1070–1079, https://doi.org/10.1016/j.ijbiomac.2020.07.085.
[24] I. Laudadio, V. Fulci, F. Palone, L. Stronati, S. Cucchiara, C. Carissimi, Quantitative assessment of shotgun metagenomics and 16S rDNA amplicon sequencing in the study of human gut microbiome, OMICS 22 (4) (2018) 248–254, https://doi.org/10.1089/omi.2018.0013.
[25] F.Z. Su, C.X. Bai, W.S. Zhang, Y.Y. Zhang, M. Liu, Y.P. Sun, B.Y. Yang, H.X. Kuang, Q.H. Wang, Polysaccharides from bile *Arisaema* exert an antipyretic effect on yeast-induced fever rats through regulating gut microbiota and metabolic profiling, Int. J. Biol. Macromol. 278 (Pt 3) (2024) 134823, https://doi.org/10.1016/j.ijbiomac.2024.134823.
[26] N. Cui, W. Zhang, F. Su, Z. Zhang, B. Li, D. Peng, Y. Sun, Y. Zeng, B. Yang, H. Kuang, Q. Wang, Metabolomic and lipidomic studies on the intervention of taurochenodeoxycholic acid in mice with hyperlipidemia, Front. Pharmacol. 14 (2023) 1255931, https://doi.org/10.3389/fphar.2023.1255931.
[27] N. Cui, W. Zhang, F. Su, Z. Zhang, W. Qiao, Y. Sun, B. Yang, H. Kuang, Q. Wang, Metabolomics and Lipidomics study unveils the impact of tauroursodeoxycholic acid on hyperlipidemic mice, Molecules 28 (17) (2023) 6352, https://doi.org/10.3390/molecules28176352.
[28] W. Zhang, N. Cui, F. Su, Y. Sun, B. Li, Z. Zhang, Y. Zeng, W. Guan, B. Yang, Q. Wang, H. Kuang, Therapeutic impact of stachyose on hyperlipidemia caused by a high-fat diet in mice as revealed by gut microbiota and metabolomics, Curr. Res. Food Sci. 7 (2023) 100638, https://doi.org/10.1016/j.crfs.2023.100638.
[29] Zhang, P., Su, F., Zhu, E., Bai, C., Zhang, B., Sun, Y., Kuang, H., Wang, Q. Exploring the lipid-lowering mechanism of *Arisaema* cum bile based on gut microbiota and metabolomics [J]. Chin. J. Tradit. Chin. Med., 1-16 10.19540/j.cnki.cjcmm.20241218.301.
[30] P. Xie, J.B. Xie, M.Y. Xiao, M. Guo, Y.S. Qi, F.F. Li, X.L. Piao, Liver lipidomics analysis reveals the anti-obesity and lipid-lowering effects of gypnosides from heat-processed Gynostemma pentaphyllum in high-fat diet fed mice, Phytomedicine 115 (2023) 154834, https://doi.org/10.1016/j.phymed.2023.154834.
[32] M.X. Li, M.Y. Li, J.X. Lei, Y.Z. Wu, Z.H. Li, L.M. Chen, C.L. Zhou, J.Y. Su, G. X. Huang, X.Q. Huang, X.B. Zheng, Huangqin decoction ameliorates DSS-induced ulcerative colitis: role of gut microbiota and amino acid metabolism, mTOR pathway and intestinal epithelial barrier, Phytomedicine 100 (2022) 154052, https://doi.org/10.1016/j.phymed.2022.154052.
[33] X. Zhang, H. Xu, J. Yu, J. Cui, Z. Chen, Y. Li, Y. Niu, S. Wang, S. Ran, Y. Zou, J. Wu, J. Xia, Immune regulation of the liver through the PCSK9/CD36 pathway during heart transplant rejection, Circulation 148 (4) (2023) 336–353, https://doi.org/10.1161/CIRCULATIONAHA.123.062788.
[34] L. Huang, Q. Rao, C. Wang, Y. Mou, X. Zheng, E. Hu, J. Zheng, Y. Li, L. Liu, Multi-omics joint analysis reveals that the Miao medicine Yindanxinnaotong formula attenuates non-alcoholic fatty liver disease, Phytomedicine 135 (2024) 156026, https://doi.org/10.1016/j.phymed.2024.156026.
[35] J. Huo, Q. Liao, J. Wu, D. Zhao, W. Sun, M. An, Y. Li, M. Huang, B. Sun, Structure elucidation and intestinal barrier protection of an α-D-glucan in Huangshui, Int. J. Biol. Macromol. 223 (Pt A) (2022) 595–605, https://doi.org/10.1016/j.ijbiomac.2022.11.059.
[36] M. Ayyash, B. Abu-Jdayil, P. Itsaranuwat, E. Galiwango, C. Tamiello-Rosa, H. Abdullah, G. Esposito, Y. Hunashal, R.S. Obaid, F. Hamed, Characterization, bioactivities, and rheological properties of exopolysaccharide produced by novel probiotic Lactobacillus plantarum C70 isolated from camel milk, Int. J. Biol. Macromol. 144 (2020) 938–946, https://doi.org/10.1016/j.ijbiomac.2019.09.171.
[37] J. Bak, B. Yoo, Rheological characteristics of concentrated ternary gum mixtures with xanthan gum, guar gum, and carboxymethyl cellulose: effect of NaCl, sucrose, pH, and temperature, Int. J. Biol. Macromol. 253 (Pt 2) (2023) 126559, https://doi.org/10.1016/j.ijbiomac.2023.126559.
[38] Y. Jing, R.X. Cao, X. Lei, Z.L. Wang, X.L. Huang, J.R. Di, Z.X. Mi, X. Zhao, M. Wang, M.M. Jiang, et al., Structural characterization of polysaccharide from the peel of Trichosanthes kirilowii maxim and its anti-hyperlipidemia activity by regulating gut microbiota and inhibiting cholesterol absorption, Bioorg. Chem. 149 (2024) 107487, https://doi.org/10.1016/j.bioorg.2024.107487.
[39] M. Chylińska, M. Szymańska-Chargot, A. Zdunek, FT-IR and FT-Raman characterization of non-cellulosic polysaccharides fractions isolated from plant cell wall, Carbohydr. Polym. 154 (2016) 48–54, https://doi.org/10.1016/j.carbpol.2016.07.121.
[40] Y. Yu, L. Cui, X. Liu, Y. Wang, C. Song, U. Pak, K.H. Mayo, L. Sun, Y. Zhou, Determining methyl-esterification patterns in plant-derived homogalacturonan pectins, Front. Nutr. 9 (2022) 925050, https://doi.org/10.3389/fnut.2022.925050.
[41] J. Liang, Y.X. Huang, X.H. Zhu, F.Y. Zhou, T.Y. Wu, J.F. Jia, X. Liu, H.X. Kuang, Y. G. Xia, Structural identification, rheological properties and immunological receptor of a complex galacturonoglucan from fruits of *Schisandra chinensis* (Turcz.) Baill, Carbohydr. Polym. 346 (2024) 122644, https://doi.org/10.1016/j.carbpol.2024.122644.
[42] X. Jia, W. Xu, L. Zhang, X. Li, R. Wang, S. Wu, Impact of gut microbiota and microbiota-related metabolites on hyperlipidemia, Front. Cell. Infect. Microbiol. 11 (2021) 634780, https://doi.org/10.3389/fcimb.2021.634780.
[43] F.Z. Su, C.X. Bai, W.S. Zhang, Y.Y. Zhang, M. Liu, Y.P. Sun, B.Y. Yang, H.X. Kuang, Q.H. Wang, Polysaccharides from bile Arisaema exert an antipyretic effect on yeast-induced fever rats through regulating gut microbiota and metabolic profiling, Int. J. Biol. Macromol. 278 (Pt 3) (2024) 134823, https://doi.org/10.1016/j.ijbiomac.2024.134823.
[44] C. Bourgneuf, D. Bailbé, A. Lamazière, C. Dupont, M. Moldes, D. Farabos, N. Roblot, C. Gauthier, E. Mathieu d'Argent, J. Cohen-Tannoudji, D. Monniaux, B. Fève, J. Movassat, N. di Clemente, C. Racine, The Goto-Kakizaki rat is a spontaneous prototypical rodent model of polycystic ovary syndrome, Nat. Commun. 12 (1) (2021) 1064, https://doi.org/10.1038/s41467-021-21308-y.
[45] J. Liang, Y.X. Huang, X.H. Zhu, F.Y. Zhou, T.Y. Wu, J.F. Jia, X. Liu, H.X. Kuang, Y. G. Xia, Structural identification, rheological properties and immunological receptor of a complex galacturonoglucan from fruits of *Schisandra chinensis* (Turcz.) Baill, Carbohydr. Polym. 346 (2024) 122644, https://doi.org/10.1016/j.carbpol.2024.122644.
[46] J.R. Speakman, Use of high-fat diets to study rodent obesity as a model of human obesity, Int. J. Obes. (Lond) 43 (8) (2019) 1491–1492, https://doi.org/10.1038/s41366-019-0363-7.
[47] E.E. Kershaw, J.S. Flier, Adipose tissue as an endocrine organ, J. Clin. Endocrinol. Metab. 89 (6) (2004) 2548–2556, https://doi.org/10.1210/jc.2004-0395.
[48] C. Priest, P. Tontonoz, Inter-organ cross-talk in metabolic syndrome, Nat. Metab. 1 (12) (2019) 1177–1188, https://doi.org/10.1038/s42255-019-0145-5.
[49] S. Kartsoli, C.E. Kostara, V. Tsimihodimos, E.T. Bairaktari, D.K. Christodoulou, Lipidomics in non-alcoholic fatty liver disease, World J. Hepatol. 12 (8) (2020) 436–450, https://doi.org/10.4254/wjh.v12.i8.436.
[50] T. Sun, X. Wang, P. Cong, J. Xu, C. Xue, Mass spectrometry-based lipidomics in food science and nutritional health: a comprehensive review, Compr. Rev. Food Sci. Food Saf. 19 (5) (2020) 2530–2558, https://doi.org/10.1111/1541-4337.12603.
[51] T. Wang, X. Fu, Q. Chen, J.K. Patra, D. Wang, Z. Wang, Z. Gai, Arachidonic acid metabolism and kidney inflammation, Int. J. Mol. Sci. 20 (15) (2019) 3683, https://doi.org/10.3390/ijms20153683.
[52] M.K. Montgomery, A.Z. Taddese, J. Bayliss, S. Nie, N.A. Williamson, M.J. Watt, Hexosaminidase A (HEXA) regulates hepatic sphingolipid and lipoprotein metabolism in mice, FASEB J. 35 (12) (2021) e22046, https://doi.org/10.1096/fj.202101186R.
[53] X. Ai, Q. Zhang, Q. Ma, M. Fang, K. Zhu, Y. Cai, Q. Yang, L. Zhang, Transcriptomics and metabolomics analysis of the pathogenesis of a novel hyperlipidemia-susceptible rat strain, Exp. Anim. 74 (2) (2025) 160–172, https://doi.org/10.1538/expanim.24-0080.
[54] N. Puig, M. Estruch, L. Jin, J.L. Sanchez-Quesada, S. Benitez, The role of distinctive sphingolipids in the inflammatory and apoptotic effects of electronegative LDL on monocytes, Biomolecules 9 (8) (2019) 300, https://doi.org/10.3390/biom9080300.
[55] J.K. Nicholson, E. Holmes, J. Kinross, R. Burcelin, G. Gibson, W. Jia, S. Pettersson, Host-gut microbiota metabolic interactions, Science 336 (6086) (2012) 1262–1267, https://doi.org/10.1126/science.1223813.

[56] C.J. Lynch, S.H. Adams, Branched-chain amino acids in metabolic signalling and insulin resistance, Nat. Rev. Endocrinol. 10 (12) (2014) 723–736, https://doi.org/10.1038/nrendo.2014.171.
[57] D.O. Mook-Kanamori, W. Römisch-Margl, G. Kastenmüller, C. Prehn, A.K. Petersen, T. Illig, C. Gieger, R. Wang-Sattler, C. Meisinger, A. Peters, J. Adamski, K. Suhre, Increased amino acids levels and the risk of developing of hypertriglyceridemia in a 7-year follow-up, J. Endocrinol. Invest. 37 (4) (2014) 369–374, https://doi.org/10.1007/s40618-013-0044-7.
[58] S. Nagaoka, H. Masaki, Y. Aoyama, A. Yoshida, Effects of excess dietary tyrosine or certain xenobiotics on the cholesterogenesis in rats, J. Nutr. 116 (5) (1986) 726–732, https://doi.org/10.1093/jn/116.5.726.
[59] M. Li, X. Shu, H. Xu, C. Zhang, L. Yang, L. Zhang, G. Ji, Integrative analysis of metabolome and gut microbiota in diet-induced hyperlipidemic rats treated with berberine compounds, J. Transl. Med. 14 (1) (2016) 237, https://doi.org/10.1186/s12967-016-0987-5.
[60] G. Czibik, Z. Mezdari, D. Murat Altintas, J. Bréhat, M. Pini, T. d'Humières, T. Delmont, C. Radu, M. Breau, H. Liang, C. Martel, A. Abatan, R. Sarwar, O. Marion, S. Naushad, Y. Zhang, M. Halfaoui, N. Suffee, D. Morin, S. Adnot, S. Hatem, A. Yavari, D. Sawaki, G. Derumeaux, Dysregulated phenylalanine catabolism plays a key role in the trajectory of cardiac aging, Circulation 144 (7) (2021) 559–574, https://doi.org/10.1161/CIRCULATIONAHA.121.054204.
[61] D. Yu, N.E. Richardson, C.L. Green, A.B. Spicer, M.E. Murphy, V. Flores, C. Jang, I. Kasza, M. Nikodemova, M.H. Wakai, J.L. Tomasiewicz, S.E. Yang, B.R. Miller, H. H. Pak, J.A. Brinkman, J.M. Rojas, W.J. Quinn, E.P. Cheng, E.N. Konon, L. R. Haider, M. Finke, M. Sonsalla, C.M. Alexander, J.D. Rabinowitz, J.A. Baur, K. C. Malecki, D.W. Lamming, The adverse metabolic effects of branched-chain amino acids are mediated by isoleucine and valine, Cell Metab. 33 (5) (2021) 905–922.e6, https://doi.org/10.1016/j.cmet.2021.03.025.
[62] L.M. França, C.F.F. Coêlho, L.N.C. Freitas, I.L.S. Souza, V.T. Chagas, V. Debbas, T. M. de Lima, H.P. de Souza, F.R.M. Laurindo, A.M.A. Paes, Syzygium cumini leaf extract reverts hypertriglyceridemia via downregulation of the hepatic XBP-1s/PDI/MTP axis in monosodium L-glutamate-induced obese rats, Oxid. Med. Cell. Longev. 2019 (2019) 9417498, https://doi.org/10.1155/2019/9417498.
[63] X. Fu, Z. Liu, R. Li, J. Yin, H. Sun, C. Zhu, Q. Kong, H. Mou, S. Nie, Amelioration of hydrolyzed guar gum on high-fat diet-induced obesity: integrated hepatic transcriptome and metabolome, Carbohydr. Polym. 297 (2022) 120051, https://doi.org/10.1016/j.carbpol.2022.120051.
[64] M. Wang, L.J. Ma, Y. Yang, Z. Xiao, J.B. Wan, n-3 Polyunsaturated fatty acids for the management of alcoholic liver disease: a critical review, Crit. Rev. Food Sci. Nutr. 59 (sup1) (2019) S116–S129, https://doi.org/10.1080/10408398.2018.1544542.
[65] A. Hirata, A. Kakino, T. Okamura, The relationship between serum levels of LOX-1 ligand containing ApoA1 as a novel marker of dysfunctional HDL and coronary artery calcification in middle-aged Japanese men [J], Atherosclerosis 313 (2020) 20–25, https://doi.org/10.1016/j.atherosclerosis.2020.09.013.
[66] M. Tsujita, B. Vaisman, L. Chengyu, K.C. Vickers, K.I. Okuhira, S. Braesch-Andersen, A.T. Remaley, Apolipoprotein A-I in mouse cerebrospinal fluid derives from the liver and intestine via plasma high-density lipoproteins assembled by ABCA1 and LCAT, FEBS Lett. 595 (6) (2021) 773–788, https://doi.org/10.1002/1873-3468.13950.
[67] W.J. Chen, W.K. Huang, S.R. Pather, W.F. Chang, L.Y. Sung, H.C. Wu, M.Y. Liao, C. C. Lee, H.H. Wu, C.Y. Wu, K.S. Liao, C.Y. Lin, S.C. Yang, H. Lin, P.L. Lai, C.H. Ng, C. M. Hu, I.C. Chen, C.H. Chuang, C.Y. Lai, P.Y. Lin, Y.C. Lee, S.C. Schuyler, A. Schambach, F.L. Lu, J. Lu, Podocalyxin-like protein 1 regulates pluripotency through the cholesterol biosynthesis pathway, Adv Sci (Weinh). 10 (1) (2022) e2205451, https://doi.org/10.1002/advs.202205451.
[68] Q. Shahzad, L. Pu, A. Ahmed Wadood, M. Waqas, L. Xie, C. Shekhar Pareek, H. Xu, X. Liang, Y. Lu, Proteomics analysis reveals that the Warburg effect along with modifications in lipid metabolism improves in vitro embryo development under low oxygen, Int. J. Mol. Sci. 21 (6) (2020) 1996, https://doi.org/10.3390/ijms21061996.
[69] L. Xiao-Rong, M. Ning, L. Xi-Wang, L. Shi-Hong, Q. Zhe, B. Li-Xia, Y. Ya-Jun, L. Jian-Yong, Untargeted and targeted metabolomics reveal the underlying mechanism of aspirin eugenol ester ameliorating rat hyperlipidemia via inhibiting FXR to induce CYP7A1, Front. Pharmacol. 12 (2021) 733789, https://doi.org/10.3389/fphar.2021.733789.
[70] M. Yan, Y. Zhao, S. Man, Y. Dai, L. Ma, W. Gao, Diosgenin as a substitute for cholesterol alleviates NAFLD by affecting CYP7A1 and NPC1L1-related pathway, Phytomedicine 125 (2024) 155299, https://doi.org/10.1016/j.phymed.2023.155299.
[71] H. Qi, Y. Li, H. Yun, T. Zhang, Y. Huang, J. Zhou, H. Yan, J. Wei, Y. Liu, Z. Zhang, Y. Gao, Y. Che, X. Su, D. Zhu, Y. Zhang, J. Zhong, R. Yang, Lactobacillus maintains healthy gut mucosa by producing L-ornithine, Commun Biol. 2 (2019) 171, https://doi.org/10.1038/s42003-019-0424-4.
[72] M.X. Li, M.Y. Li, J.X. Lei, Y.Z. Wu, Z.H. Li, L.M. Chen, C.L. Zhou, J.Y. Su, G. X. Huang, X.Q. Huang, X.B. Zheng, Huangqin decoction ameliorates DSS-induced ulcerative colitis: role of gut microbiota and amino acid metabolism, mTOR pathway and intestinal epithelial barrier, Phytomedicine 100 (2022) 154052, https://doi.org/10.1016/j.phymed.2022.154052.
[73] C. Chen, S. Fang, H. Wei, M. He, H. Fu, X. Xiong, Y. Zhou, J. Wu, J. Gao, H. Yang, L. Huang, Prevotella copri increases fat accumulation in pigs fed with formula diets, Microbiome 9 (1) (2021) 175, https://doi.org/10.1186/s40168-021-01110-0.
[74] L. Hu, Y. Xu, J. Li, M. Zhang, Z. Sun, Y. Ban, X. Tian, D. Liu, L. Hu, Gut microbiome characteristics of women with hypothyroidism during early pregnancy detected by 16S rRNA amplicon sequencing and shotgun metagenomic, Front. Cell. Infect. Microbiol. (14) (2024) 1369192, https://doi.org/10.3389/fcimb.2024.1369192.
[75] X. Zhang, O.O. Coker, E.S. Chu, K. Fu, H.C.H. Lau, Y.X. Wang, A.W.H. Chan, H. Wei, X. Yang, J.J.Y. Sung, J. Yu, Dietary cholesterol drives fatty liver-associated liver cancer by modulating gut microbiota and metabolites, Gut 70 (4) (2021) 761–774, https://doi.org/10.1136/gutjnl-2019-319664.
[76] K. Deng, M. Shuai, Z. Zhang, Z. Jiang, Y. Fu, L. Shen, J.S. Zheng, Y.M. Chen, Temporal relationship among adiposity, gut microbiota, and insulin resistance in a longitudinal human cohort, BMC Med. 20 (1) (2022) 171, https://doi.org/10.1186/s12916-022-02376-3.
[77] H.T. Chen, J.S. Li, J. Li, L. Li, Z.C. Xu, Y. Zhang, R.R. Wang, *Lactobacillus murinus*: a key factor in suppression of enterogenous *Candida albicans* infections in compound agrimony enteritis capsules-treated mice, J. Ethnopharmacol. 311 (2023) 116361, https://doi.org/10.1016/j.jep.2023.116361.
[78] L.F. Li, H.W. Zou, B.L. Song, Y. Wang, Y. Jiang, Z.L. Li, Q.H. Niu, Y.J. Liu, Increased Lactobacillus abundance contributes to stress resilience in mice exposed to chronic social defeat stress, Neuroendocrinology 113 (5) (2023) 563–576, https://doi.org/10.1159/000528876.
[79] S. Yue, C. Peng, D. Zhao, X. Xia, C. Tan, Q. Wang, J. Gong, Theabrownin isolated from Pu-erh tea regulates Bacteroidetes to improve metabolic syndrome of rats induced by high-fat, high-sugar and high-salt diet, J. Sci. Food Agric. 102 (10) (2022) 4250–4265, https://doi.org/10.1002/jsfa.11777.
[80] N. Kei, K.K. Cheung, K.L. Ma, T.K. Yau, S. Lauw, V.W.S. Wong, L. You, P.C. K. Cheung, Effects of oat β-glucan and inulin on alleviation of nonalcoholic steatohepatitis aggravated by circadian disruption in C57BL/6J mice, J. Agric. Food Chem. 72 (7) (2024) 3520–3535, https://doi.org/10.1021/acs.jafc.3c08028.
[81] X. Zhu, J. Cai, Y. Wang, X. Liu, X. Chen, H. Wang, Z. Wu, W. Bao, H. Fan, S. Wu, A high-fat diet increases the characteristics of gut microbial composition and the intestinal damage associated with non-alcoholic fatty liver disease, Int. J. Mol. Sci. 24 (23) (2023) 16733, https://doi.org/10.3390/ijms242316733.